Journal of Scientific Computing (2025) 103:90
https://doi.org/10.1007/s10915-025-02898-x

Traveling-Wave Solutions and Structure-Preserving Numerical Methods for a Hyperbolic Approximation of the Korteweg-de Vries Equation

Abhijit Biswas[1] · **David I. Ketcheson**[1] · **Hendrik Ranocha**[2] · **Jochen Schütz**[3]

Received: 23 December 2024 / Revised: 20 March 2025 / Accepted: 22 March 2025

Abstract
We study the recently-proposed hyperbolic approximation of the Korteweg-de Vries equation (KdV). We show that this approximation, which we call KdVH, possesses a rich variety of solutions, including solitary wave solutions that approximate KdV solitons, as well as other solitary and periodic solutions that are related to higher-order water wave models, and may include singularities. We analyze a class of implicit–explicit Runge–Kutta time discretizations for KdVH that are asymptotic preserving, energy conserving, and can be applied to other hyperbolized systems. We also develop structure-preserving spatial discretizations based on summation-by-parts operators in space including finite difference, discontinuous Galerkin, and Fourier methods. We use the entropy relaxation approach to make the fully discrete schemes energy-preserving. Numerical experiments demonstrate the effectiveness of these discretizations.

Keywords Hyperbolic approximation · Traveling-wave · Asymptotic-preserving · Asymptotic-accuracy · Energy-conserving · Summation-by-parts · Finite-difference · Implicit–explicit Runge–Kutta (ImEx-RK) methods

Mathematics Subject Classification 65L04 · 65L20 · 65M06 · 65M12 · 65M22

✉ Abhijit Biswas
abhijit.biswas@kaust.edu.sa

David I. Ketcheson
david.ketcheson@kaust.edu.sa

Hendrik Ranocha
hendrik.ranocha@uni-mainz.de

Jochen Schütz
jochen.schuetz@uhasselt.be

[1] Computer, Electrical, and Mathematical Sciences and Engineering Division, King Abdullah University of Science and Technology, Thuwal 23955, Saudi Arabia

[2] Institute of Mathematics, Johannes Gutenberg University Mainz, Mainz, Germany

[3] Faculty of Sciences and Data Science Institute, Hasselt University, Hasselt, Belgium

Published online: 05 May 2025

1 Introduction

The Korteweg-de Vries equation (KdV)

$$\partial_t \eta + \eta \partial_x \eta + \partial_x^3 \eta = 0 \tag{1}$$

is a widely studied model for water waves and perhaps the simplest known nonlinear integrable partial differential equation (PDE) [54]. A hyperbolic approximation of KdV, referred to herein as KdVH, has been proposed recently [4]:

$$\partial_t u + u \partial_x u + \partial_x w = 0 \,, \tag{2a}$$

$$\tau \partial_t v = (\partial_x v - w) \,, \tag{2b}$$

$$\tau \partial_t w = -(\partial_x u - v) \,. \tag{2c}$$

here $\tau > 0$ is referred to as the relaxation parameter. When $\tau \to 0$ (referred to as the *relaxation limit*), formally one obtains $v \to u_x$ and $w \to u_{xx}$ so that (2a) becomes equivalent to (1) with $u \to \eta$.

Similar hyperbolic approximations have been proposed for a number of other dispersive nonlinear wave equations [2, 3, 12, 13, 19, 23, 24, 28, 29, 41] as well as other classes of PDEs [18, 20, 27, 39, 49, 52]. A general approach to such approximations has been given in [36]. The KdVH system (2) was proposed with the idea of facilitating the implementation of accurate nonreflecting boundary conditions in an approximation of the KdV Eq. [4]. In that work, the authors also briefly analyzed the dispersion relation, hyperbolic structure, and one class of traveling wave solutions. They presented numerical solutions obtained with 2nd-order operator splitting in time and a 2nd-order MUSCL scheme in space.

In this work we further study the structure and numerical discretization of the KdVH system (2). In Sect. 2 we perform a more complete study of traveling wave solutions of KdVH. The KdV equation admits soliton solutions of arbitrary large height and speed. Nevertheless, such waves beyond a certain height are known to be unphysical [10]. The KdVH system imposes a maximum speed on such soliton-like waves and therefore avoids, at least qualitatively, this non-physical aspect of the KdV model (see further discussion in Sect. 2). We will also see that the KdVH system has traveling waves that are related to solutions of the Camassa-Holm system [11], in which solutions are known to propagate at finite speed in a certain sense [14].

Given the many special properties of KdV (1), it is natural to ask whether or to what extent they are preserved by (2). It is also desirable to develop numerical discretizations of (2) that preserve this structure at the discrete level. In Sect. 3, we develop high-order accurate time and space discretizations that are asymptotic preserving and that exactly preserve a quadratic invariant. We present results on asymptotic preservation for Implicit–explicit (ImEx) Runge–Kutta methods under a range of assumptions. In Sect. 4 we present numerical examples that support the theoretical results and demonstrate the effectiveness of this approach for approximating solutions of the KdV Eq. (1).

The new contributions of the present work include:

- Characterization of the limits of soliton-like traveling wave solutions;
- Identification and analysis of other traveling wave solutions, including some with no counterpart in KdV but that seem to be related to other water wave models;
- Efficient ImEx time integration methods that are provably asymptotic preserving and asymptotically accurate;
- Energy-preserving full discretizations based on summation-by-parts operators in space and entropy relaxation in time.

2 Traveling Wave Solutions of KdVH

In this section we study traveling wave solutions of the KdVH system, focusing first on waves that approximate KdV solitons in Sect. 2.1 and then on a variety of other classes of traveling waves in Sect. 2.2. The calculations in this section were performed using the Python packages NumPy [30], SciPy [53], and Matplotlib [31].

2.1 KdV-Soliton-Like Waves

The soliton solutions of the KdV Eq. (1) take the form

$$\eta(x,t) = 3c\,\mathrm{sech}^2\left(\frac{\sqrt{9c}(x-ct)}{6}\right). \tag{3}$$

The parameter c, which controls the width, amplitude, and speed of these waves, can take any positive value. Thus, the KdV equation possesses traveling wave solutions with arbitrarily large velocity.[1] This is perhaps not surprising, since the phase velocity of small perturbations is also unbounded with respect to the wavenumber, for the KdV equation.

Now we turn to the KdVH system. To find traveling wave solutions, we apply the *ansatz*

$$u = \tilde{u}(x-ct) \qquad v = \tilde{v}(x-ct) \qquad w = \tilde{w}(x-ct) \tag{4}$$

and we furthermore assume that each dependent variable tends to a constant as $|\xi| := |x - ct| \to \infty$. Then from (2) we obtain the ordinary differential equation (ODE) system

$$-c\tilde{u}' + \tilde{w}' + \tilde{u}\tilde{u}' = 0 \tag{5a}$$
$$-c\tau\tilde{v}' = \tilde{v}' - \tilde{w} \tag{5b}$$
$$-c\tau\tilde{w}' = -\tilde{u}' + \tilde{v}. \tag{5c}$$

We integrate the first equation and assume that $\tilde{u}$, $\tilde{w}$ tend to zero for large $|x - ct|$ in order to determine the constant of integration. We substitute the result into the other two equations above to obtain the system

$$\tilde{u}' = \frac{1}{1 + c\tau(\tilde{u} - c)}\tilde{v} \tag{6a}$$
$$\tilde{v}' = \frac{1}{1 + c\tau}(c - \tilde{u}/2)\tilde{u}. \tag{6b}$$

As depicted in Fig. 1, this system has two equilibrium points: $(\tilde{u}, \tilde{v}) = (0, 0)$ and $(\tilde{u}, \tilde{v}) = (2c, 0)$. For $\tau^{-1} > c^2$, the origin is a hyperbolic point, while the other equilibrium is always a center, with

$$H(\tilde{u}, \tilde{v}) = \frac{\tilde{v}^2}{2} - \frac{\tilde{u}^2}{1 + c\tau}\left(-\frac{c\tau}{8}\tilde{u}^2 + \frac{3c^2\tau - 1}{6}\tilde{u} + \frac{c\left(1 - c^2\tau\right)}{2}\right)$$

as a first integral of the system. The system has a homoclinic connection (along the level set $H(\tilde{u}, \tilde{v}) = 0$), corresponding to a solitary wave. Figure 1 shows the phase portrait of the system (6), along with a solitary wave solution obtained by numerically integrating (6). This structure is essentially the same as that found when studying traveling wave solutions of the

[1] In addition to the soliton solutions, there also exist periodic traveling wave solutions of KdV with any positive velocity.

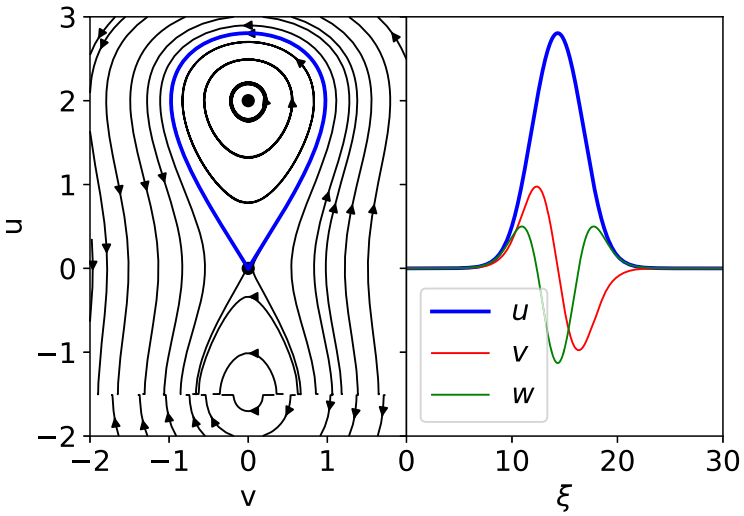

Fig. 1 Phase portrait of the KdVH traveling wave system (6) with wave speed $c = 1$ and relaxation parameter $\tau = 2/5$. The homoclinic orbit, shown in blue, begins and ends at the saddle point $(0, 0)$, corresponding to a solitary traveling wave solution. These waves tend to KdV solitons in the limit $\tau \to 0$. Note the presence of a line singularity, where the denominator in (6a) vanishes

KdV equation, and the homoclinic orbit tends to a KdV soliton as $\tau \to 0$. Even though the relaxation parameter is not very small for the case plotted here, one can easily see that for this solution $v \approx u_x$ and $w \approx v_x$.

In order to compute these solitary waves more accurately, we use a Petviashvili-type algorithm [1]. We rewrite (6) as a single second-order ODE for $\tilde{u}$. Differentiating (6a) gives

$$\tilde{v}' = (1 + c\tau(\tilde{u} - c))\tilde{u}'' + c\tau(\tilde{u}')^2.$$

Substituting this in (6b), we obtain after some simplification

$$(1 - c^2\tau)\tilde{u}'' + c\tau\tilde{u}\tilde{u}'' + c\tau(\tilde{u}')^2 = \tilde{u}\frac{c - \tilde{u}/2}{1 + c\tau}.$$

This can be further rewritten as

$$-\tilde{u}'' + \frac{c}{(1 + c\tau)(1 - c^2\tau)}\tilde{u} = \frac{1}{(1 + c\tau)(1 - c^2\tau)}\frac{\tilde{u}^2}{2} + \frac{c\tau}{1 - c^2\tau}\left(\tilde{u}\tilde{u}'\right)'. \tag{7}$$

Note that as $\tau \to 0$, (7) formally converges to

$$-\tilde{u}'' + c\tilde{u} = \frac{\tilde{u}^2}{2},$$

the equation satisfied by traveling waves of the KdV equation. Next we write 7) in the form $L\tilde{u} = N(\tilde{u})$, where the linear operator is given by $L = -D^2 + \frac{c}{(1+c\tau)(1-c^2\tau)}I$, (with D the derivative operator); and the nonlinear operator is defined as $N(\tilde{u}) = \frac{1}{(1+c\tau)(1-c^2\tau)}\frac{\tilde{u}^2}{2} + \frac{c\tau}{1-c^2\tau}\left(\tilde{u}\tilde{u}'\right)'$. Next we discretize, approximating the derivative operator D using Fourier spectral differentiation. Then we iteratively solve the system

$$Lu^{[k+1]} = m\left(u^{[k]}\right)^2 N\left(u^{[k]}\right), \quad k = 0, 1, 2, \ldots$$

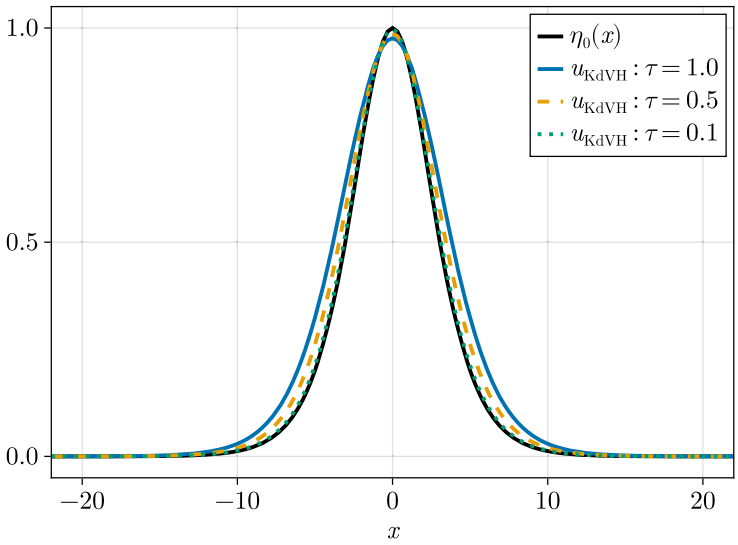

Fig. 2 Comparison of the analytical soliton solution (3) (denoted by $\eta_0(x)$) of the KdV equation and the numerical solitary waves (denoted by $u_{\mathrm{KdVH}} : \tau$) for the KdVH system with different relaxation parameters τ and $c = \frac{1}{3}$. The solutions of the KdVH system converge to the exact solutions of the KdV equation as $\tau \to 0$, which is clearly evident

where $u^{[0]}$ is an initial guess and $m(u^n) = \frac{\langle Lu^n, u^n \rangle}{\langle N(u^n), u^n \rangle}$ is the stabilizing factor.

Choosing the domain $[-30\pi, 30\pi]$ with 2^9 spatial grid points, we compute the solitary waves of the KdVH system for three different values of the relaxation parameter: $\tau = 1.0, 0.5, 0.1$ using the Petviashvili algorithm. We iterate until the residual $\|Lu^{[k]} - N(u^{[k]})\|_\infty$ is approximately machine precision (for IEEE 64-bit floating point numbers). Figure 2 displays the resulting numerical KdVH solitary waves and the corresponding KdV soliton (3). We see that the KdVH solitary waves converge to the soliton as $\tau \to 0$.

The KdVH system also possesses periodic traveling waves with finite period (not shown here), which tend to the well-known cnoidal solutions of the KdV equation as $\tau \to 0$.

However, this does not fully describe the dynamics of the system (6). Notably, for $c^2 > \tau^{-1}$, the origin is not a saddle; instead the eigenvalues of the Jacobian are purely imaginary. Correspondingly, there is no homoclinic connection originating from the origin. Furthermore, as can be seen in the left plot of Fig. 1, system (6) becomes singular when $\tilde{u}$ is chosen such that the denominator of (6a) vanishes. These observations hint at the existence of other, quite different traveling waves, which we study in the next section.

2.2 Other Traveling Wave Solutions

It turns out that the KdVH system admits a much larger set of traveling wave solutions, some of which seem to be related to other dispersive water wave models. To investigate general traveling waves, we note from (4) that such a wave with speed c must satisfy

$$v_t + cv_x = 0$$
$$w_t + cw_x = 0.$$

These two equations stem from the representation of traveling waves, and are as such independent of the actual form of the KdVH equation. Subsituting $-cv_x$ and $-cw_x$, respectively, for v_t and w_t, respectively, into (2b) and (2c), one obtains

$$v = u_x - \alpha w_x \tag{8a}$$

$$w = (1+\alpha)v_x, \tag{8b}$$

where $\alpha = c\tau$.

Substituting v_x in (8b) through $u_{xx} - \alpha w_{xx}$, derived from (8a), we end up with the equation

$$w + \alpha(1+\alpha)w_{xx} \equiv \left(I + \alpha(1+\alpha)\partial_x^2\right) w = (1+\alpha)u_{xx}. \tag{9}$$

Together with the requirement that w is a smooth function that vanishes at $x = \pm\infty$, this constitutes a well-posed problem in w and hence allows for a unique solution w as a function of the right-hand side. The spatial derivative of said function is given by

$$w_x = \left(I + \alpha(1+\alpha)\partial_x^2\right)^{-1} u_{xxx}. \tag{10}$$

Substituting in (2a), we obtain the dispersive equation

$$u_t + uu_x + (1+\alpha)(I + \alpha(1+\alpha)\partial_x^2)^{-1}u_{xxx} = 0,$$

or equivalently (upon multiplication by $(I + \alpha(1+\alpha)\partial_x^2)$)

$$u_t + uu_x + (1+\alpha)u_{xxx} + \alpha(1+\alpha)(u_{xxt} + 3u_x u_{xx} + uu_{xxx}) = 0. \tag{11}$$

As $\alpha \to 0$ we formally recover the KdV equation, as expected, and if we apply the ansatz (4) we find an ODE system equivalent to (6). Indeed, this analysis is in a sense equivalent to that of (4)–(6) above, but it is revealing since (11) involves the same set of terms as the integrable Camassa-Holm and Degasperis-Procesi equations. It is not possible to transform (11) exactly into either of those systems (see [15, Dfns. 1–2],[2]), but it is natural to expect that traveling wave solutions of KdVH may include waves that are similar in nature to solutions of the Camassa-Holm or Degasperis-Procesi equations, and in fact this is the case.

Some examples of these traveling waves are shown in Fig. 3a–d. These include waves with arbitrarily large positive speed, as well as left-going solitary waves that have very nearly the shape of $\sqrt{\operatorname{sech} x}$, quite different from KdV solitons. Furthermore, they include sharply-peaked solutions that are homoclinic connections originating from a point on the line of singularity. These solutions have no counterpart in solutions of KdV but seem to be related to solutions of the Degasperis-Procesi or Camassa-Holm equations.

Remark 1 For $c\tau > 0$ (i.e., for right-going solutions of KdVH), the coefficient of u_{xxt} in (11) is positive. This may seem problematic, since the linearization of (11) is ill-posed in this case. However, it should be remembered that not all solutions of (11) are solutions of (2); we additionally require that there exist a consistent solution of (8), which is equivalent to

$$v + \alpha(1+\alpha)v_{xx} = u_x$$
$$w + \alpha(1+\alpha)w_{xx} = (1+\alpha)u_{xx}.$$

In experiments we have conducted (not shown here), these waves are not observed to spontaneously emerge from general initial data, even if the initial data is not well-prepared. However, using any of these traveling wave solutions as initial data, we observe that they are dynamically stable for long times.

[2] However, (11) does belong to the class of equations described in [15, Prop. 2] which approximate the Serre-Green-Naghdi equations.

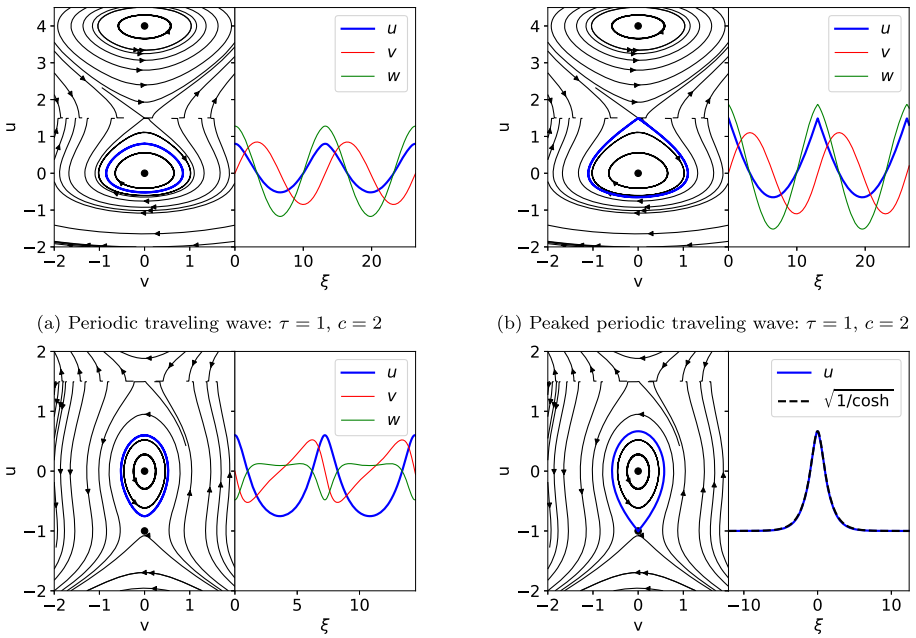

(a) Periodic traveling wave: $\tau = 1$, $c = 2$

(b) Peaked periodic traveling wave: $\tau = 1$, $c = 2$

(c) Periodic traveling wave: $\tau = 1$, $c = -1/2$

(d) Solitary wave: $\tau = 1$, $c = -1/2$

Fig. 3 Traveling wave solutions of the KdVH equation. These solutions have no counterpart in KdV solutions. Waves in the top row travel to the right at a speed greater than what is possible for soliton-like traveling waves. Waves in the bottom row travel to the left. The bottom-right solitary wave has nearly (but not quite) the shape $(5/3)\sqrt{\operatorname{sech}(5x/3)} - 1$, which is plotted for comparison. Note the presence of a line singularity, where the denominator in (6a) vanishes

Remark 2 The KdVH system can be written as a hyperbolic balance law

$$q_t + F'(q)q_x = S(q). \tag{12}$$

The eigenvalues of the flux Jacobian $F'(q)$ evaluated at $u = 0$ are $-\tau^{-1}, \pm\tau^{-1/2}$. Notice that the greatest eigenvalue $+\sqrt{1/\tau}$ coincides precisely with the maximum speed of the soliton-like traveling waves from the previous section.

3 Asymptotic-Preserving and Energy-Conserving Numerical Discretization

In this section we develop structure-preserving discretizations for the KdVH system (2), focusing primarily on ImEx Runge–Kutta (RK) methods. Let $q^n = [u^n, v^n, w^n]^T$ and $q^{n+1} = [u^{n+1}, v^{n+1}, w^{n+1}]^T$ denote the numerical approximation of the solution at time t_n and $t_{n+1} = t_n + \Delta t$, respectively. Starting from the solution q^n at time t_n, an ImEx-RK method applied to the system

$$q_t = f(q) + g(q)$$

computes the approximate solution at time t_{n+1} as

$$q^{(i)} = q^n + \Delta t \left(\sum_{j=1}^{i-1} \tilde{a}_{ij} f(q^{(j)}) + \sum_{j=1}^{i} a_{ij} g(q^{(j)}) \right), \ i = 1, 2, \ldots, s \,, \tag{13a}$$

$$q^{n+1} = q^n + \Delta t \left(\sum_{j=1}^{s} \tilde{b}_j f(q^{(j)}) + \sum_{j=1}^{s} b_j g(q^{(j)}) \right) \,. \tag{13b}$$

This method can be compactly represented by the following Butcher tableau:

$$\begin{array}{c|c} \tilde{\boldsymbol{c}} & \tilde{A} \\ \hline & \tilde{\boldsymbol{b}}^T \end{array} \qquad \begin{array}{c|c} \boldsymbol{c} & A \\ \hline & \boldsymbol{b}^T \end{array} \,, \tag{14}$$

where the matrix $\tilde{A} = (\tilde{a}_{ij}) \in \mathbb{R}^{s\times s}$ represents the explicit part, $A = (a_{ij}) \in \mathbb{R}^{s\times s}$ represents the implicit part, and the vectors $\tilde{\boldsymbol{c}}$, $\tilde{\boldsymbol{b}}$, $\boldsymbol{c}$, and $\boldsymbol{b}$ are in $\mathbb{R}^s$. The choice of the splitting between the functions f and g is a key element of the schemes introduced below.

3.1 Asymptotic-Preserving Time Discretization

The KdVH system (2) includes both convective and algebraic terms that depend on the relaxation parameter τ and become arbitrarily stiff as $\tau \to 0$. To deal with this stiffness we include the stiff terms in g, to be integrated implicitly. Our goal is to obtain accurate numerical solutions for all values of τ. In particular we seek a numerical discretization that tends to a consistent discretization of KdV as $\tau \to 0$; this is known as an *asymptotic-preserving (AP)* scheme [9, 33]. In the rest of this section, we investigate the AP property for different classes of ImEx schemes. In Sect. 4 we provide numerical tests that confirm the theoretical results.

The AP schemes provide an efficient methodology for solving multi-scale relaxation problems. We denote the continuous problem (2) with the parameter τ as P^τ, and its limiting problem, which reduces to the KdV equation, as P^0. For the development of AP schemes, it is sufficient to focus initially on time discretization, leaving space continuous for now, with suitable spatial discretization to be adopted later. To this end, we denote by P_h^τ the numerical discretization of the continuous problem P^τ, where h represents the discretization parameters. For instance, $h = \Delta t$ denotes the time step in a problem that is continuous in space, or $h = (\Delta t, \Delta x)$ in the fully discrete case. The AP property guarantees that for fixed discretization parameters h, the scheme P_h^τ provides, in the limit $\tau \to 0$, a consistent discretization of the limit problem P^0, denoted by P_h^0. This relationship is summarized in Fig. 4. Our primary focus in this section is on the limit $P_h^\tau \to P_h^0$ of the numerical discretizations, although we will also comment on the convergence of the methods for $h \to 0$.

The AP property can be defined in general as follows:

Definition 1 We say the numerical discretization P_h^τ is AP if the limiting discretization $P_h^0 = \lim_{\tau\to 0} P_h^\tau$ is a consistent and stable discretization of the continuous limit model P^0.

The AP property does not ensure that the scheme retains its order of accuracy in the stiff limit $\tau \to 0$; for that we use the term *asymptotically-accurate* (AA).

Definition 2 The numerical discretization P_h^τ is AA if the local truncation error of P_h^τ with respect to P^τ is the same as that of P_h^0 with respect to P^0.

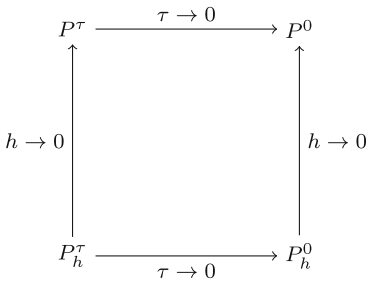

Fig. 4 A schematic illustration of the AP property [32]

The design of an AP ImEx scheme requires careful selection of the terms to be integrated implicitly or explicitly. It might seem most natural to separate the hyperbolic terms from the algebraic (source) terms, but this turns out not to provide the AP property. Here we propose a different splitting that facilitates the construction of AP schemes. Namely, we integrate explicitly only the nonlinear convective term, and integrate implicitly all of the remaining (linear) terms:

$$\underbrace{\begin{pmatrix} u \\ v \\ w \end{pmatrix}_t}_{=q_t} = \underbrace{\begin{pmatrix} -uu_x \\ 0 \\ 0 \end{pmatrix}}_{=f(q)} + \underbrace{\begin{pmatrix} -w_x \\ \frac{1}{\tau}(v_x - w) \\ \frac{1}{\tau}(-u_x + v) \end{pmatrix}}_{=g(q)}. \tag{15}$$

Although the term w_x may not seem to be stiff, recall that in the relaxation limit it approximates the stiff third-derivative term. Also, including this term in g ensures that the system $q_t + g_x = 0$ is strictly hyperbolic, which is an important property with respect to stability [50, 55].

Given this splitting, we will next establish the AP property for some ImEx RK methods. To do so, we use the following specification of the AP property:

Definition 3 We say an ImEx RK method (13) applied to the splitting (15) of the KdVH system is AP for the u-component if $u^{n+1} \to \eta^{n+1}$ for $\tau \to 0$, where η^{n+1} is the numerical solution of the KdV equation with splitting

$$\eta_t = \underbrace{-\eta\eta_x}_{=f(\eta)} \underbrace{-\eta_{xxx}}_{=g(\eta)} \tag{16}$$

and the same ImEx RK method. We say it is AP for the auxiliary components v and w if $v^{n+1} \to \eta_x^{n+1}$ and $w^{n+1} \to \eta_{xx}^{n+1}$ for $\tau \to 0$.

We now establish the AP property and provide sufficient conditions for the AA property for our proposed splitting of the KdVH system using two classes of additive Runge–Kutta (ARK) methods — type I (also known as type A) and type II (also known as type CK) [9]. An ImEx-RK method is classified as type I if the matrix $A \in \mathbb{R}^{s\times s}$ is invertible. An ARK method is of type II if $a_{11} = 0$, in which case it can be written as

$$\begin{array}{c|cc} 0 & 0 & \\ \hat{\tilde{\boldsymbol{c}}} & \hat{\tilde{\boldsymbol{a}}} & \hat{\tilde{A}} \\ \hline & \hat{\tilde{b}}_1 & \hat{\tilde{\boldsymbol{b}}}^T \end{array} \qquad \begin{array}{c|cc} 0 & 0 & \\ \hat{\boldsymbol{c}} & \hat{\boldsymbol{a}} & \hat{A} \\ \hline & \hat{b}_1 & \hat{\boldsymbol{b}}^T \end{array}. \tag{17}$$

here $\hat{\tilde{\boldsymbol{c}}}, \hat{\tilde{\boldsymbol{a}}}, \hat{\tilde{\boldsymbol{b}}}, \hat{\boldsymbol{c}}, \hat{\boldsymbol{a}}$, and $\hat{\boldsymbol{b}}$ are vectors in $\mathbb{R}^{s-1}$, $\hat{\tilde{b}}_1$ and $\hat{b}_1$ are scalars in $\mathbb{R}$, and $\hat{\tilde{A}}$, $\hat{A}$ are matrices in $\mathbb{R}^{(s-1)\times(s-1)}$, where $\hat{A}$ is assumed to be invertible and lower-triangular, so that the method is diagonally implicit.

This analysis, depending on the method class, involves two additional conditions [9]. An ImEx-RK method is said to be *globally stiffly accurate* (GSA) if

$$\tilde{a}_{si} = \tilde{b}_i \quad \text{and} \quad a_{si} = b_i, \quad i = 1, 2, \ldots, s. \tag{18}$$

Thus, the implicit part is stiffly accurate (SA) and the explicit part has a first-same-as-last (FSAL) structure.

The initial data for KdVH (2) is said to be *well-prepared* if $v(x, 0) = Du$ and $w(x, 0) = D^2u$. Here $D = \partial_x$ in the present section, where we consider solutions continuous in space. For a fully discrete scheme, D should be replaced by the discrete derivative used in the scheme.

The proofs and results below are similar to those in the literature for other classes of relaxation systems [9]. However, the relaxation system considered here, with the specific splitting (15), differs in such a way that the AP property cannot be deduced directly from previous results.

We now present the following results regarding the AP and AA properties of type I methods:

Theorem 1 *An ImEx-RK method of type I applied to the splitting (15) of the hyperbolic approximation of the KdV equation is always AP for the u-component. For such a method, in the stiff limit $\tau \to 0$, we have*

$$u^{n+1} - \eta(t_{n+1}) = \mathcal{O}(\Delta t^p) \,, \tag{19}$$

where p is the order of the ImEx-RK method. Furthermore, if the method is assumed to be globally stiffly accurate, it is also AP for the auxiliary components v and w. In the stiff limit $\tau \to 0$, we have

$$v^{n+1} - \eta_x(t_{n+1}) = \mathcal{O}(\Delta t^p) \quad \textit{and} \quad w^{n+1} - \eta_{xx}(t_{n+1}) = \mathcal{O}(\Delta t^p) \,. \tag{20}$$

Proof Let us denote by $\boldsymbol{u} = [u^{(1)}, u^{(2)}, \ldots, u^{(s)}]^T$, $\boldsymbol{v} = [v^{(1)}, v^{(2)}, \ldots, v^{(s)}]^T$, and $\boldsymbol{w} = [w^{(1)}, w^{(2)}, \ldots, w^{(s)}]^T$ the vectors of stage-solution components for the variables u, v, and w, respectively, and let $\boldsymbol{e} = [1, 1, \ldots, 1]^T$ be the vector of ones in $\mathbb{R}^s$. For the KdVH system with the splitting (15), the Eq. (13a) in component form becomes

$$\boldsymbol{u} = u^n \boldsymbol{e} + \Delta t \left(\tilde{A}(-\boldsymbol{u}\boldsymbol{u}_x) + A(-\boldsymbol{w}_x) \right) \,, \tag{21a}$$

$$\boldsymbol{v} = v^n \boldsymbol{e} + \frac{\Delta t}{\tau} A(\boldsymbol{v}_x - \boldsymbol{w}) \,, \tag{21b}$$

$$\boldsymbol{w} = w^n \boldsymbol{e} + \frac{\Delta t}{\tau} A(-\boldsymbol{u}_x + \boldsymbol{v}) \,. \tag{21c}$$

Similarly, the final update of the solution can be written in components as

$$u^{n+1} = u^n + \Delta t \left(\tilde{\boldsymbol{b}}^T(-\boldsymbol{u}\boldsymbol{u}_x) + \boldsymbol{b}^T(-\boldsymbol{w}_x) \right) \,, \tag{22a}$$

$$v^{n+1} = v^n + \frac{\Delta t}{\tau} \boldsymbol{b}^T(\boldsymbol{v}_x - \boldsymbol{w}) \,, \tag{22b}$$

$$w^{n+1} = w^n + \frac{\Delta t}{\tau} \boldsymbol{b}^T(-\boldsymbol{u}_x + \boldsymbol{v}) \,. \tag{22c}$$

We assume there exist Hilbert expansions for u^n, v^n, and w^n:

$$u^n = u_0^n + \tau u_1^n + \tau^2 u_2^n + \cdots, \quad v^n = v_0^n + \tau v_1^n + \tau^2 v_2^n + \cdots,$$
$$w^n = w_0^n + \tau w_1^n + \tau^2 w_2^n + \cdots, \tag{23}$$

and for the stage vectors $\boldsymbol{u}$, $\boldsymbol{v}$, and $\boldsymbol{w}$ of the stage solution components:

$$\boldsymbol{u} = \boldsymbol{u}_0 + \tau \boldsymbol{u}_1 + \tau^2 \boldsymbol{u}_2 + \cdots, \quad \boldsymbol{v} = \boldsymbol{v}_0 + \tau \boldsymbol{v}_1 + \tau^2 \boldsymbol{v}_2 + \cdots,$$
$$\boldsymbol{w} = \boldsymbol{w}_0 + \tau \boldsymbol{w}_1 + \tau^2 \boldsymbol{w}_2 + \cdots.$$

We insert these expansions into the stage equations and compare the leading-order terms in the powers of τ. The leading-order terms in the expansions for the stage Eqs. (21b) and (21c) yield:

$$\mathcal{O}\left(\tau^{-1}\right): \begin{cases} A\left((\boldsymbol{v}_0)_x - \boldsymbol{w}_0\right) = \boldsymbol{0}, \\ A\left(-(\boldsymbol{u}_0)_x + \boldsymbol{v}_0\right) = \boldsymbol{0}. \end{cases}$$

Since A is invertible, it follows that

$$\boldsymbol{v}_0 = (\boldsymbol{u}_0)_x \quad \text{and} \quad \boldsymbol{w}_0 = (\boldsymbol{v}_0)_x. \tag{24}$$

The leading-order term in the expansion of (21a) gives

$$\mathcal{O}\left(\tau^0\right): \boldsymbol{u}_0 = u_0^n \boldsymbol{e} + \Delta t \left(-\tilde{A}\boldsymbol{u}_0(\boldsymbol{u}_0)_x - A(\boldsymbol{w}_0)_x\right).$$

Using $\boldsymbol{v}_0 = (\boldsymbol{u}_0)_x$ and $\boldsymbol{w}_0 = (\boldsymbol{v}_0)_x$ in the previous equation, we obtain

$$\boldsymbol{u}_0 = u_0^n \boldsymbol{e} + \Delta t \left(-\tilde{A}\boldsymbol{u}_0(\boldsymbol{u}_0)_x - A(\boldsymbol{u}_0)_{xxx}\right). \tag{25}$$

Using the Eq. (24) in the leading-order term of the solution update for the first equation yields:

$$u_0^{n+1} = u_0^n + \Delta t \left(-\tilde{\boldsymbol{b}}^T \boldsymbol{u}_0(\boldsymbol{u}_0)_x - \boldsymbol{b}^T(\boldsymbol{u}_0)_{xxx}\right). \tag{26}$$

In the limit as $\tau \to 0$ the numerical scheme becomes:

$$\boldsymbol{u}_0 = u_0^n \boldsymbol{e} + \Delta t \left(-\tilde{A}\boldsymbol{u}_0(\boldsymbol{u}_0)_x - A(\boldsymbol{u}_0)_{xxx}\right),$$
$$u_0^{n+1} = u_0^n + \Delta t \left(-\tilde{\boldsymbol{b}}^T \boldsymbol{u}_0(\boldsymbol{u}_0)_x - \boldsymbol{b}^T(\boldsymbol{u}_0)_{xxx}\right).$$

This is precisely the numerical scheme obtained from the time-stepping method (14) of type I when applied to the KdV equation $\eta_t = -\eta\eta_x - \eta_{xxx}$, where the term $-\eta\eta_x$ is treated explicitly and the term $-\eta_{xxx}$ is treated implicitly. Thus, we also have $u^{n+1} - \eta(t_{n+1}) = \mathcal{O}(\Delta t^p)$, where p is the order of the ImEx-RK method.

In addition if the method is GSA then we can prove the AP property for the auxiliary variables v and w. To prove this, we use the Eqs. (21b) and (21c). By utilizing the invertibility of A, we obtain the following:

$$\frac{\Delta t}{\tau}(\boldsymbol{v}_x - \boldsymbol{w}) = A^{-1}\left(\boldsymbol{v} - v^n \boldsymbol{e}\right),$$
$$\frac{\Delta t}{\tau}(-\boldsymbol{u}_x + \boldsymbol{v}) = A^{-1}\left(\boldsymbol{w} - w^n \boldsymbol{e}\right).$$

Inserting these expressions into the update rules for the auxiliary components, (22b) and (22c), we obtain:

$$v^{n+1} = v^n + \boldsymbol{b}^T A^{-1}\left(\boldsymbol{v} - v^n \boldsymbol{e}\right) = \boldsymbol{b}^T A^{-1}\boldsymbol{v} + \left(1 - \boldsymbol{b}^T A^{-1}\boldsymbol{e}\right) v^n \,,$$
$$w^{n+1} = w^n + \boldsymbol{b}^T A^{-1}\left(\boldsymbol{w} - w^n \boldsymbol{e}\right) = \boldsymbol{b}^T A^{-1}\boldsymbol{w} + \left(1 - \boldsymbol{b}^T A^{-1}\boldsymbol{e}\right) w^n \,.$$

Since the method is assumed to be GSA, the stiff accuracy of A implies that $\boldsymbol{b}^T A^{-1} = [0, 0, \ldots, 1]$ in $\mathbb{R}^s$, hence $1 - \boldsymbol{b}^T A^{-1}\boldsymbol{e} = 0$. Using this information, we obtain:

$$v^{n+1} = \boldsymbol{b}^T A^{-1}\boldsymbol{v} = v^{(s)} \,,$$
$$w^{n+1} = \boldsymbol{b}^T A^{-1}\boldsymbol{w} = w^{(s)} \,.$$

In the limit as $\tau \to 0$, we have $v_0^{n+1} = v_0^{(s)}$ and $w_0^{n+1} = w_0^{(s)}$. Using Eq. (24), we can express $v_0^{n+1} = (u_0^{(s)})_x$ and $w_0^{n+1} = (u_0^{(s)})_{xx}$. By the GSA property of the scheme, it follows from Eqs. (25) and (26) that $u_0^{(s)} = u_0^{n+1}$, which leads to $v_0^{n+1} = (u_0^{n+1})_x$ and $w_0^{n+1} = (u_0^{n+1})_{xx}$. This establishes the AP property of the type I ImEx-RK method for the auxiliary components. In the stiff limit $\tau \to 0$, the following error estimates hold for the v and w components:

$$v^{n+1} - \eta_x(t_{n+1}) = \mathcal{O}(\Delta t^p) \text{ and } w^{n+1} - \eta_{xx}(t_{n+1}) = \mathcal{O}(\Delta t^p).$$

□

Remark 3 Without the GSA assumption in Theorem 1, the AP property is obtained only for the u-component. In this case, the auxiliary variables may not remain on the manifold of equilibria, which could lead to a degradation in their accuracy. However, this does not affect the order of accuracy of the u-component.

We now consider ImEx-RK methods of type II and prove the AP property for these methods. Before establishing the results for a general method in this class, we first examine the asymptotic-preserving property of the simple type II method ARS(1,1,1) when applied to the splitting (15). The ARS(1,1,1) method updates the solution from time step t^n to t^{n+1} as follows:

$$q^{n+1} = q^n + \Delta t f\left(q^n\right) + \Delta t g\left(q^{n+1}\right),$$

where the components of the update are given by:

$$u^{n+1} = u^n + \Delta t\left(-u^n u_x^n - w_x^{n+1}\right) \,, \tag{31a}$$
$$v^{n+1} = v^n + \frac{\Delta t}{\tau}\left(v_x^{n+1} - w^{n+1}\right) \,, \tag{31b}$$
$$w^{n+1} = w^n + \frac{\Delta t}{\tau}\left(-u_x^{n+1} + v^{n+1}\right) \,. \tag{31c}$$

We now insert the Hilbert expansions (23) into the updating equations and analyze the leading-order term in the expansions in terms of τ. The leading-order terms in expansions of Eqs. (31b) and (31c) yield

$$\mathcal{O}\left(\tau^{-1}\right)\colon\ w_0^{n+1} = (v_0^{n+1})_x \quad \text{and} \quad v_0^{n+1} = \left(u_0^{n+1}\right)_x \,.$$

The Eq. (31a) implies

$$\mathcal{O}\left(\tau^0\right): u_0^{n+1} = u_0^n - \Delta t u_0^n (u_0^n)_x - \Delta t \left(w_0^{n+1}\right)_x .$$

Using $w_0^{n+1} = (v_0^{n+1})_x$ and $v_0^{n+1} = (u_0^{n+1})_x$ in the previous equation, we obtain

$$u_0^{n+1} = u_0^n - \Delta t u_0^n (u_0^n)_x - \Delta t \left(u_0^{n+1}\right)_{xxx} ,$$

$$\frac{u_0^{n+1} - u_0^n}{\Delta t} + u_0^n (u_0^n)_x + \left(u_0^{n+1}\right)_{xxx} = 0 ,$$

which, in the limit $\tau \to 0$, is the discretization of the original KdV equation by the ARS(1,1,1) method. This proves the AP property of the ARS(1,1,1) method for the splitting (15). To prove the AP property for a general ImEx-RK method of type II, we require an additional assumption of well-preparedness of the initial data. The well-preparedness of the initial data for our system, following [9], is given by

$$v^0 = u_x^0 + \mathcal{O}(\tau) \quad \text{and} \quad w^0 = u_{xx}^0 + \mathcal{O}(\tau). \tag{32}$$

For a general ImEx-RK method of type II, we prove the following result:

Theorem 2 *A globally stiffly accurate ImEx-RK method of type II, applied to the splitting (15) of the hyperbolic approximation of the KdV equation, together with the well-prepared initial data (32), is AP for all components u, v, and w. Furthermore, in the stiff limit $\tau \to 0$, the following error estimates apply to all components:*

$$u^{n+1} - \eta(t_{n+1}) = \mathcal{O}(\Delta t^p), \;\; v^{n+1} - \eta_x(t_{n+1}) = \mathcal{O}(\Delta t^p), \text{ and } w^{n+1} - \eta_{xx}(t_{n+1}) = \mathcal{O}(\Delta t^p) ,$$

where p is the order of the ImEx-RK method.

Proof Let $q^n = [u^n, v^n, w^n]^T$ and $q^{n+1} = [u^{n+1}, v^{n+1}, w^{n+1}]^T$ denote the numerical approximations to the true solution at time t_n and $t_{n+1} = t_n + \Delta t$, respectively. Starting from the solution q^n at time t_n, an ImEx-RK method of type II (17) applied to the system

$$q_t = f(q) + g(q)$$

computes the approximate solution at time t_{n+1} as

$$q^{(1)} = q^n , \tag{33a}$$

$$q^{(i)} = q^n + \Delta t \left(\hat{\tilde{a}}_{i1} f(q^n) + \sum_{j=2}^{i-1} \hat{\tilde{a}}_{ij} f\left(q^{(j)}\right) + \hat{a}_{i1} g(q^n) + \sum_{j=2}^{i} \hat{a}_{ij} g\left(q^{(j)}\right) \right) ,$$

$$i = 2, 3, \ldots, s , \tag{33b}$$

$$q^{n+1} = q^n + \Delta t \left(\hat{\tilde{b}}_1 f(q^n) + \sum_{j=2}^{s} \hat{\tilde{b}}_j f\left(q^{(j)}\right) + \hat{b}_1 g(q^n) + \sum_{j=2}^{s} \hat{b}_j g\left(q^{(j)}\right) \right) . \tag{33c}$$

Using the notation $\boldsymbol{q} = [q^{(2)}, q^{(3)}, \ldots, q^{(s)}]^T$, the identity matrix I in $\mathbb{R}^{3\times 3}$, and the vector of ones $\boldsymbol{e}$ in $\mathbb{R}^{s-1}$, this can be written compactly as

$$\boldsymbol{q} = \boldsymbol{e} \otimes q^n + \Delta t \left(\hat{\tilde{\boldsymbol{a}}} \otimes f(q^n) + \left(\hat{\tilde{A}} \otimes I \right) f(\boldsymbol{q}) + \hat{\boldsymbol{a}} \otimes g(q^n) + \left(\hat{A} \otimes I \right) g(\boldsymbol{q}) \right) , \tag{34a}$$

$$q^{n+1} = q^n + \Delta t \left(\hat{\tilde{b}}_1 f(q^n) + \left(\hat{\tilde{\boldsymbol{b}}}^T \otimes I \right) f(\boldsymbol{q}) + \hat{b}_1 g(q^n) + \left(\hat{\boldsymbol{b}}^T \otimes I \right) g(\boldsymbol{q}) \right) . \tag{34b}$$

Let us denote by $\boldsymbol{u} = [u^{(2)}, u^{(3)}, \dots, u^{(s)}]^T$, $\boldsymbol{v} = [v^{(2)}, v^{(3)}, \dots, v^{(s)}]^T$, and $\boldsymbol{w} = [w^{(2)}, w^{(3)}, \dots, w^{(s)}]^T$ the vectors of stage-solution components for the variables u, v, and w, respectively. For the KdVH system with the splitting (15), the Eq. (34a) in component form becomes

$$\boldsymbol{u} = u^n \boldsymbol{e} + \Delta t \left(\left(-u^n u_x^n \right) \hat{\hat{\boldsymbol{a}}} + \hat{\hat{A}}(-\boldsymbol{u}\boldsymbol{u}_x) - w_x^n \hat{\boldsymbol{a}} + \hat{A}(-\boldsymbol{w}_x) \right) , \tag{35a}$$

$$\boldsymbol{v} = v^n \boldsymbol{e} + \frac{\Delta t}{\tau} \left((v_x^n - w^n) \hat{\boldsymbol{a}} + \hat{A}(\boldsymbol{v}_x - \boldsymbol{w}) \right) , \tag{35b}$$

$$\boldsymbol{w} = w^n \boldsymbol{e} + \frac{\Delta t}{\tau} \left((-u_x^n + v^n) \hat{\boldsymbol{a}} + \hat{A}(-\boldsymbol{u}_x + \boldsymbol{v}) \right) . \tag{35c}$$

Similarly, the final update of the solution can be written in components as

$$u^{n+1} = u^n + \Delta t \left(\hat{\hat{b}}_1 (-u^n u_x^n) + \hat{\hat{\boldsymbol{b}}}^T (-\boldsymbol{u}\boldsymbol{u}_x) + \hat{b}_1 (-w_x^n) + \hat{\boldsymbol{b}}^T (-\boldsymbol{w}_x) \right) , \tag{36a}$$

$$v^{n+1} = v^n + \frac{\Delta t}{\tau} \left(\hat{b}_1 (v_x^n - w^n) + \hat{\boldsymbol{b}}^T (\boldsymbol{v}_x - \boldsymbol{w}) \right) , \tag{36b}$$

$$w^{n+1} = w^n + \frac{\Delta t}{\tau} \left(\hat{b}_1 (-u_x^n + v^n) + \hat{\boldsymbol{b}}^T (-\boldsymbol{u}_x + \boldsymbol{v}) \right) . \tag{36c}$$

We assume there exist Hilbert expansions (23) for u^n, v^n, and w^n and similar expansions for the stage vectors $\boldsymbol{u}$, $\boldsymbol{v}$, and $\boldsymbol{w}$ of the stage solution components:

$$\boldsymbol{u} = \boldsymbol{u}_0 + \tau \boldsymbol{u}_1 + \tau^2 \boldsymbol{u}_2 + \cdots , \quad \boldsymbol{v} = \boldsymbol{v}_0 + \tau \boldsymbol{v}_1 + \tau^2 \boldsymbol{v}_2 + \cdots ,$$
$$\boldsymbol{w} = \boldsymbol{w}_0 + \tau \boldsymbol{w}_1 + \tau^2 \boldsymbol{w}_2 + \cdots .$$

We insert these expansions into the stage equations and compare the leading-order terms in the powers of τ. The leading-order terms in the expansions for the stage Eqs. (35b) and (35c) yield:

$$\mathcal{O}\left(\tau^{-1}\right): \begin{cases} \left((v_0^n)_x - w_0^n \right) \hat{\boldsymbol{a}} + \hat{A} \left((\boldsymbol{v}_0)_x - \boldsymbol{w}_0 \right) = \boldsymbol{0} , \\ \left(-(u_0^n)_x + v_0^n \right) \hat{\boldsymbol{a}} + \hat{A} \left(-(\boldsymbol{u}_0)_x + \boldsymbol{v}_0 \right) = \boldsymbol{0} . \end{cases}$$

The well-prepared initial data at time t_n implies that $v_0^n = (u_0^n)_x$ and $w_0^n = (v_0^n)_x$. Since $\hat{A}$ is invertible, it follows that

$$\boldsymbol{v}_0 = (\boldsymbol{u}_0)_x \quad \text{and} \quad \boldsymbol{w}_0 = (\boldsymbol{v}_0)_x . \tag{37}$$

The leading-order term in the expansion of (35a) gives

$$\mathcal{O}\left(\tau^0\right): \boldsymbol{u}_0 = u_0^n \boldsymbol{e} + \Delta t \left(-u_0^n (u_0^n)_x \hat{\hat{\boldsymbol{a}}} - \hat{\hat{A}} \boldsymbol{u}_0 (\boldsymbol{u}_0)_x - (w_0^n)_x \hat{\boldsymbol{a}} - \hat{A} (\boldsymbol{w}_0)_x \right) .$$

Using $\boldsymbol{v}_0 = (\boldsymbol{u}_0)_x$, $\boldsymbol{w}_0 = (\boldsymbol{v}_0)_x$, and the well-preparedness of the initial data at time t_n in the previous equation, we obtain

$$\boldsymbol{u}_0 = u_0^n \boldsymbol{e} + \Delta t \left(-u_0^n (u_0^n)_x \hat{\hat{\boldsymbol{a}}} - \hat{\hat{A}} \boldsymbol{u}_0 (\boldsymbol{u}_0)_x - (u_0^n)_{xxx} \hat{\boldsymbol{a}} - \hat{A} (\boldsymbol{u}_0)_{xxx} \right) . \tag{38}$$

The solution update for the first equation in the leading-order term becomes:

$$u_0^{n+1} = u_0^n + \Delta t \left(-\hat{\hat{b}}_1 u_0^n (u_0^n)_x - \hat{\hat{\boldsymbol{b}}}^T \boldsymbol{u}_0 (\boldsymbol{u}_0)_x - \hat{b}_1 (u_0^n)_{xxx} - \hat{\boldsymbol{b}}^T (\boldsymbol{u}_0)_{xxx} \right) . \tag{39}$$

In the limit as $\tau \to 0$, we have $u^n = u_0^n$ and $\boldsymbol{u} = \boldsymbol{u}_0$, so the numerical scheme becomes:

$$\boldsymbol{u}_0 = u_0^n \boldsymbol{e} + \Delta t \left(-u_0^n (u_0^n)_x \hat{\tilde{\boldsymbol{a}}} - \hat{\tilde{A}} \boldsymbol{u}_0 (\boldsymbol{u}_0)_x - (u_0^n)_{xxx} \hat{\boldsymbol{a}} - \hat{A} (\boldsymbol{u}_0)_{xxx} \right) ,$$

$$u_0^{n+1} = u_0^n + \Delta t \left(-\hat{\tilde{b}}_1 u_0^n (u_0^n)_x - \hat{\tilde{\boldsymbol{b}}}^T \boldsymbol{u}_0 (\boldsymbol{u}_0)_x - \hat{b}_1 (u_0^n)_{xxx} - \hat{\boldsymbol{b}}^T (\boldsymbol{u}_0)_{xxx} \right) .$$

This is precisely the numerical scheme obtained from the time-stepping method (17) when applied to the KdV equation $\eta_t = -\eta\eta_x - \eta_{xxx}$, where the term $-\eta\eta_x$ is treated explicitly and the term $-\eta_{xxx}$ is treated implicitly. It is important to note that, in order to preserve this result at the subsequent time step, the auxiliary components must remain well-prepared. Therefore, we must project v^{n+1} and w^{n+1} onto the corresponding equilibrium manifolds. To achieve this, we utilize the GSA property of the method. Since the method is assumed to satisfy the GSA property, it follows that:

$$v^{n+1} = \hat{\boldsymbol{b}}^T \hat{A}^{-1} \boldsymbol{v} = v^{(s)} ,$$

$$w^{n+1} = \hat{\boldsymbol{b}}^T \hat{A}^{-1} \boldsymbol{w} = w^{(s)} .$$

In the limit as $\tau \to 0$, we have $v_0^{n+1} = v_0^{(s)}$ and $w_0^{n+1} = w_0^{(s)}$. Using Eq. (37), we can express $v_0^{n+1} = (u_0^{(s)})_x$ and $w_0^{n+1} = (u_0^{(s)})_{xx}$. By the GSA property of the scheme, it follows from Eqs. (38) and (39) that $u_0^{(s)} = u_0^{n+1}$, which leads to $v_0^{n+1} = (u_0^{n+1})_x$ and $w_0^{n+1} = (u_0^{n+1})_{xx}$. This establishes the AP property, and the error estimates for all components follow trivially, thereby proving the AA property of the method. □

Remark 4 Note that the well-preparedness of the initial data is assumed at time t_n. This is justified by the fact that if the initial condition is well-prepared, as given by (32), then Theorem 2 for $n = 0$ ensures that the solution is well-prepared for the step $n = 1$. Hence, by an induction argument, the auxiliary components will remain on the local equilibrium for all subsequent times. Additionally, note that the GSA property is necessary to guarantee that the auxiliary variables lie on the local equilibrium manifolds, which ensures the accuracy of the u-components and, consequently, the auxiliary components.

3.2 Energy-Conserving Spatial Semidiscretization

As a completely integrable nonlinear PDE, the KdV equation possesses an infinite set of conserved quantities, can be derived from a Lagrangian or Hamiltonian formalism, and possesses soliton solutions that are related to certain symmetries. Here we review these properties and related properties of the KdVH system.

Consider the Lagrangian

$$L = -\frac{\phi_t \phi_x}{2} - \frac{(\phi_x)^3}{6} - \frac{\phi_x \phi_{xxx}}{2} .$$

The corresponding Euler-Lagrange equation is

$$\phi_{xt} + \phi_x \phi_{xx} + \phi_{xxxx} = 0 .$$

Introducing the variable $\eta = \phi_x$, we obtain the KdV Eq. (1).

As noted in the appendix of [4], the KdVH system (2) can also be derived from a variational principle, starting from the augmented Lagrangian

$$\hat{L} = -\frac{\phi_t \phi_x}{2} - \frac{\phi_x^3}{6} - \phi_x \chi_x - \tau \frac{\chi_t \chi_x}{2} - \tau \frac{\psi_t \psi_x}{2} + \frac{\psi_x^2}{2} + \psi \chi_x . \tag{42}$$

The corresponding Euler-Lagrange equations are

$$\begin{aligned}
&\phi_{xt} + \phi_x \phi_{xx} + \chi_{xx} = 0 \,, \\
&\tau \psi_{xt} - \psi_{xx} + \chi_x = 0 \,, \\
&\tau \chi_{xt} + \phi_{xx} - \psi_x = 0 \,.
\end{aligned}$$

Setting $u = \phi_x$, $v = \psi_x$, and $w = \chi_x$, we recover the hyperbolized system (2).

Similarly, the KdVH system (2) can be expressed as a Hamiltonian PDE; the Hamiltonian is obtained from the augmented Lagrangian (42) using the Legendre transformation. This yields the Hamiltonian density:

$$\begin{aligned}
\mathcal{H}(\phi, \psi, \chi, \phi_x, \psi_x, \chi_x) &= \frac{\partial \hat{L}}{\partial \phi_t}\phi_t + \frac{\partial \hat{L}}{\partial \psi_t}\psi_t + \frac{\partial \hat{L}}{\partial \chi_t}\chi_t - \hat{L} \\
&= \frac{\phi_x^3}{6} + \phi_x \chi_x - \psi \chi_x - \frac{\psi_x^2}{2} \,.
\end{aligned}$$

In terms of u, v, and w, this is

$$H(u, v, w) = \int_{x_L}^{x_R} \left(\frac{u^3}{6} + uw - wF(v) - \frac{v^2}{2} \right) dx \,, \tag{44}$$

where

$$F(v)(x, t) = \int_{x_L}^{x} v(y, t) dy \,.$$

Then the KdVH system can be expressed in the form $q_t = \mathcal{J}\delta H(q)$ where $q = [u, v, w]^T$ and

$$\delta H(q) = \begin{bmatrix} \frac{u^2}{2} + w \\ -v + F(w) \\ u - F(v) \end{bmatrix} \qquad \mathcal{J} = \begin{bmatrix} -\partial_x & & \\ & -\frac{\partial_x}{\tau} & \\ & & -\frac{\partial_x}{\tau} \end{bmatrix} \,, \tag{45}$$

the KdV hyperbolized system (2) can be expressed in the Hamiltonian PDE form $q_t = \mathcal{J}\delta H(q)$.

The first three conserved quantities of the KdV Eq. (1) are

$$\int \eta \, dx \quad \text{(mass)}, \tag{46a}$$

$$\int \frac{1}{2}\eta^2 \, dx \quad \text{(energy)}, \tag{46b}$$

$$\int \left(2\eta^3 - \eta_x^2\right) dx \quad \text{(Whitham)}. \tag{46c}$$

For the KdVH system, it can be verified that the mass is conserved but the other nonlinear invariants are not exactly conserved. However, the system conserves a modified energy:

$$I(u, v, w) = \int_{x_L}^{x_R} \left(\frac{u^2}{2} + \tau \frac{v^2}{2} + \tau \frac{w^2}{2} \right) dx \,, \tag{47}$$

which satisfies $-q_x = \mathcal{J}\delta I(q)$ and hence we obtain the relative equilibrium structure of the Hamiltonian PDE [21, 22]. Thus, this modified energy is a conserved quantity of the KdVH

system (2). It can also be easily verified that the modified energy given in (47) is a conserved quantity of the system by checking that

$$\begin{aligned}\frac{dI}{dt} &= \int_{x_L}^{x_R} (uu_t + \tau v v_t + \tau w w_t)\, dx \\ &= \int_{x_L}^{x_R} (u(-uu_x - w_x) + v(v_x - w) + w(v - u_x))\, dx \\ &= \int_{x_L}^{x_R} \left(-\left(\frac{u^3}{3}\right)_x - (uw)_x + \left(\frac{v^2}{2}\right)_x \right) dx \\ &= 0\,.\end{aligned}$$

Formally, the modified energy (47) converges to the KdV energy for $\tau \to 0$.

Conservation of the modified energy (47) of KdVH and the original energy (46) of KdV can be shown using integration by parts and a split form of the nonlinear term, similar to Burgers' equation [48, Eq. (6.40)]. Alternatively, the chain rule can be used. However, the chain rule does not have a discrete equivalent in general [43]. Thus, we use the first approach and mimic integration by parts discretely using summation-by-parts (SBP) operators [25, 51]. In this article, we only need periodic SBP operators; see [46] and references cited therein for several examples and details.

Definition 4 A *periodic first-derivative SBP operator* consists of a grid $\boldsymbol{x}$, a consistent first-derivative operator D, and a symmetric and positive-definite matrix M such that

$$MD + D^T M = 0. \tag{48}$$

The operator D is skew-symmetric with respect to the mass matrix M. In other words, the product MD is skew-symmetric in the usual sense. In particular, $\boldsymbol{y}^T MD\boldsymbol{y} = 0$ for any vector $\boldsymbol{y}$. We will use this property several times to analyze energy conservation and refer to it as the SBP property (48).

We will also use upwind operators following [40].

Definition 5 A *periodic first-derivative upwind SBP operator* consists of a grid $\boldsymbol{x}$, consistent first-derivative operators $D_\pm$, and a symmetric and positive-definite matrix M such that

$$MD_+ + D_-^T M = 0, \quad \frac{1}{2}M(D_+ - D_-) \text{ is negative semidefinite.} \tag{49}$$

For upwind SBP operators, the arithmetic average $D = (D_+ + D_-)/2$ is an SBP operator [40]. The semidiscretizations using SBP operators use a collocation approach, i.e., all nonlinear operations are performed pointwise. For example, $\boldsymbol{u} = \big(u(\boldsymbol{x}_i)\big)_{i=1}^N$ is the vector of the values of the function u at the grid points and $\boldsymbol{u}^2 = \big(u(\boldsymbol{x}_i)^2\big)_{i=1}^N$. We will only use diagonal-norm operators, i.e., operators with diagonal mass/norm matrix M.

Example 1 First-order accurate periodic first-derivative finite difference SBP operators are given by

$$
D_+ = \frac{1}{\Delta x}\begin{pmatrix} -1 & 1 & 0 & \cdots & 0 \\ 0 & -1 & 1 & \cdots & 0 \\ \vdots & \vdots & \vdots & \ddots & \vdots \\ 0 & 0 & \cdots & -1 & 1 \\ 1 & 0 & \cdots & 0 & -1 \end{pmatrix}, \quad D_- = \frac{1}{\Delta x}\begin{pmatrix} 1 & 0 & \cdots & 0 & -1 \\ -1 & 1 & 0 & \cdots & 0 \\ 0 & -1 & 1 & \cdots & 0 \\ \vdots & \vdots & \vdots & \ddots & \vdots \\ 0 & 0 & \cdots & -1 & 1 \end{pmatrix},
$$

$$
D = \frac{D_+ + D_-}{2} = \frac{1}{2\Delta x}\begin{pmatrix} 0 & 1 & 0 & \cdots & -1 \\ -1 & 0 & 1 & \cdots & 0 \\ 0 & -1 & 0 & \cdots & 1 \\ \vdots & \vdots & \vdots & \ddots & \vdots \\ 1 & 0 & \cdots & -1 & 0 \end{pmatrix},
$$

$$
M = \Delta x\, \mathrm{I}, \tag{50}
$$

where Δx is the grid spacing and I is the identity matrix. The central SBP operator D is actually second-order accurate. Moreover,

$$
D_+ D D_- = \frac{1}{\Delta x^3}\begin{pmatrix} 0 & -1 & 1/2 & 0 & \dots & 0 & -1/2 & 1 \\ 1 & 0 & -1 & 1/2 & \dots & 0 & 0 & -1/2 \\ -1/2 & 1 & 0 & -1 & \dots & 0 & 0 & 0 \\ 0 & -1/2 & 1 & 0 & \dots & 0 & 0 & 0 \\ \vdots & \vdots & \vdots & \vdots & \ddots & \vdots & \vdots & \vdots \\ 0 & 0 & 0 & 0 & \dots & 0 & -1 & 1/2 \\ 1/2 & 0 & 0 & 0 & \dots & 1 & 0 & -1 \\ -1 & 1/2 & 0 & 0 & \dots & -1/2 & 1 & 0 \end{pmatrix} \tag{51}
$$

is a second-order accurate approximation of the third derivative.

Using the split-form discretization of the nonlinear term together with an upwind discretization of the third derivative leads to the semidiscretization

$$
\partial_t \boldsymbol{\eta} + \frac{1}{3}\left(D\boldsymbol{\eta}^2 + \boldsymbol{\eta} D\boldsymbol{\eta}\right) + D_+ D D_- \boldsymbol{\eta} = \mathbf{0} \tag{52}
$$

of the KDV Eq. (1).

Theorem 3 *The semidiscretization* (52) *conserves the discrete counterparts*

$$
\mathbf{1}^T M \boldsymbol{\eta} \approx \int \eta, \qquad \frac{1}{2}\mathbf{1}^T M \boldsymbol{\eta}^2 \approx \frac{1}{2}\int \eta^2 \tag{53}
$$

of the linear and quadratic invariant (46) of the KdV Eq. (1) *if periodic diagonal-norm upwind SBP operators with the same mass matrix M are used.*

Proof The linear invariant is conserved since

$$
\begin{aligned}
\partial_t \mathbf{1}^T M \boldsymbol{\eta} &= \mathbf{1}^T M \partial_t \boldsymbol{\eta} = -\frac{1}{3}\mathbf{1}^T M D \boldsymbol{\eta}^2 - \frac{1}{3}\mathbf{1}^T M \boldsymbol{\eta} D \boldsymbol{\eta} - \mathbf{1}^T M D_+ D D_- \boldsymbol{\eta} \\
&= -\frac{1}{3}\mathbf{1}^T M D \boldsymbol{\eta}^2 - \frac{1}{3}\boldsymbol{\eta}^T M D \boldsymbol{\eta} - \mathbf{1}^T M D_+ D D_- \boldsymbol{\eta} \\
&= +\frac{1}{3}\mathbf{1}^T D^T M \boldsymbol{\eta}^2 - \frac{1}{6}\boldsymbol{\eta}^T M D \boldsymbol{\eta} + \frac{1}{6}\boldsymbol{\eta}^T D^T M \boldsymbol{\eta} + \mathbf{1}^T D_-^T M D D_- \boldsymbol{\eta} = 0.
\end{aligned} \tag{54}
$$

In the second line, we have used that the mass matrix M is diagonal. The SBP properties are used in the third line. Please note that we have used the SBP property (48) for half of the term $-\frac{1}{3}\boldsymbol{\eta}^T M D\boldsymbol{\eta}$. The final step follows from consistency of the derivative operators ($D\mathbf{1} = \mathbf{0}$) and the symmetry of M. Finally, we obtain

$$\partial_t \mathbf{1}^T M\boldsymbol{\eta}^2 = \partial_t\left(\boldsymbol{\eta}^T M\boldsymbol{\eta}\right) = 2\boldsymbol{\eta}^T M\partial_t\boldsymbol{\eta}, \tag{55}$$

where we have used that M is diagonal. Then, we have

$$\begin{aligned}\frac{1}{2}\partial_t \mathbf{1}^T M\boldsymbol{\eta}^2 &= -\frac{1}{3}\boldsymbol{\eta}^T MD\boldsymbol{\eta}^2 - \frac{1}{3}\boldsymbol{\eta}^T M\boldsymbol{\eta} D\boldsymbol{\eta} - \boldsymbol{\eta}^T MD_+DD_-\boldsymbol{\eta}\\ &= -\frac{1}{3}\boldsymbol{\eta}^T MD\boldsymbol{\eta}^2 - \frac{1}{3}(\boldsymbol{\eta}^2)^T MD\boldsymbol{\eta} + \boldsymbol{\eta}^T D_-^T MDD_-\boldsymbol{\eta} = 0,\end{aligned} \tag{56}$$

where we have again used the SBP properties (48) and (49) in the last line and the fact that $\boldsymbol{y}^T MD\boldsymbol{y} = 0$, i.e., that MD is skew-symmetric in the usual sense. □

Next, we consider the semidiscretization

$$\begin{aligned}&\partial_t\boldsymbol{u} + \frac{1}{3}\left(D\boldsymbol{u}^2 + \boldsymbol{u}D\boldsymbol{u}\right) + D_+\boldsymbol{w} = \mathbf{0},\\ &\partial_t\boldsymbol{v} + \frac{1}{\tau}\left(-D\boldsymbol{v} + \boldsymbol{w}\right) = \mathbf{0},\\ &\partial_t\boldsymbol{w} + \frac{1}{\tau}\left(D_-\boldsymbol{u} - \boldsymbol{v}\right) = \mathbf{0}\end{aligned} \tag{57}$$

of the KdVH system (2).

Theorem 4 *The semidiscretization* (57) *conserves the discrete counterparts*

$$\mathbf{1}^T M\boldsymbol{u} \approx \int u, \qquad \frac{1}{2}\mathbf{1}^T M\left(\boldsymbol{u}^2 + \tau\boldsymbol{v}^2 + \tau\boldsymbol{w}^2\right) \approx \frac{1}{2}\int\left(u^2 + \tau v^2 + \tau w^2\right) \tag{58}$$

of the linear and quadratic invariant (47) *of the KdVH system 2 if periodic diagonal-norm upwind SBP operators with the same mass matrix M are used.*

Proof Conservation of the linear invariant follows as in the proof of Theorem 3. The quadratic invariant is conserved since

$$\begin{aligned}\frac{1}{2}\partial_t \mathbf{1}^T M\left(\boldsymbol{u}^2 + \tau\boldsymbol{v}^2 + \tau\boldsymbol{w}^2\right) &= \boldsymbol{u}^T M\partial_t\boldsymbol{u} + \tau\boldsymbol{v}^T M\partial_t\boldsymbol{v} + \tau\boldsymbol{w}^T M\partial_t\boldsymbol{w}\\ &= -\frac{1}{3}\boldsymbol{u}^T MD\boldsymbol{u}^2 - \frac{1}{3}\boldsymbol{u}^T M\boldsymbol{u}D\boldsymbol{u} - \boldsymbol{u}^T MD_+\boldsymbol{w} + \boldsymbol{v}^T MD\boldsymbol{v} - \boldsymbol{v}^T M\boldsymbol{w} - \boldsymbol{w}^T MD_-\boldsymbol{u} + \boldsymbol{w}^T M\boldsymbol{v}\\ &= -\frac{1}{3}\boldsymbol{u}^T MD\boldsymbol{u}^2 - \frac{1}{3}(\boldsymbol{u}^2)^T MD\boldsymbol{u} - \boldsymbol{u}^T MD_+\boldsymbol{w} + \boldsymbol{v}^T MD\boldsymbol{v} + \boldsymbol{w}^T D_+^T M\boldsymbol{u} = 0,\end{aligned} \tag{59}$$

where we have used that M is diagonal and the SBP properties, in particular the skew-symmetry of MD. □

Formally taking the limit $\tau \to 0$, the semidiscretization (57) of the KdVH system (2) converges to the semidiscretization (52) of the KdV Eq. (1). Moreover, the quadratic invariant of the KdVH semidiscretization converges to the quadratic invariant of the KdV semidiscretization. We can use this to prove fully-discrete counterparts of Theorems 1 and 2. Thus,

we introduce the splitting

$$\underbrace{\partial_t \begin{pmatrix} \boldsymbol{u} \\ \boldsymbol{v} \\ \boldsymbol{w} \end{pmatrix}}_{\partial_t \boldsymbol{q}} = \underbrace{\begin{pmatrix} -\frac{1}{3}\left(D\boldsymbol{u}^2 + \boldsymbol{u}D\boldsymbol{u}\right) \\ \boldsymbol{0} \\ \boldsymbol{0} \end{pmatrix}}_{f(\boldsymbol{q})} + \underbrace{\begin{pmatrix} -D_+\boldsymbol{w} \\ \frac{1}{\tau}(D\boldsymbol{v} - \boldsymbol{w}) \\ \frac{1}{\tau}(-D_-\boldsymbol{u} + \boldsymbol{v}) \end{pmatrix}}_{g(\boldsymbol{q})}. \tag{60}$$

Theorem 5 *An ImEx-RK method of type I applied to the splitting* (60) *of the semidiscrete hyperbolic approximation of the KdV equation is always AP for the* $\boldsymbol{u}$*-component. Furthermore, if the method is assumed to be globally stiffly accurate, then it is also AP for the auxiliary components* $\boldsymbol{v}$ *and* $\boldsymbol{w}$*.*

Theorem 6 *A globally stiffly accurate ImEx-RK method of type II, applied to the splitting* (60) *of the semidiscrete hyperbolic approximation of the KdV equation, along with well-prepared initial data, is asymptotic-preserving for all the components* $\boldsymbol{u}$*,* $\boldsymbol{v}$*, and* $\boldsymbol{w}$*.*

The proofs of Theorems 5 and 6 are analogous to the proofs of Theorems 1 and 2. Thus, we omit them here.

3.3 Fully-Discrete Energy Conservation via RK Relaxation

To extend energy conservation from the semidiscrete to the fully-discrete level, we utilize the entropy relaxation Runge–Kutta technique [35, 45, 47]. This approach modifies standard RK methods to conserve a single invariant for ODE systems. Applications of this entropy relaxation approach in ImEx time integration for conserving single or multiple invariants have been explored in [6, 7, 38]. Here, we focus on conserving a single invariant at the fully-discrete level using ImEx RK methods. The energy-conserving spatial semidiscretization of the KdVH or the original KdV equation reduces the problem to an ODE system for $q \in \mathbb{R}^m$, given by

$$q_t = f(q) + g(q), \quad q(0) = q^0,$$

with the energy invariant denoted by $I(q)$. Using an ImEx method (13), we require $I(q^{n+1}) = I(q^n) = I(q^0)$ at the discrete level. However, standard methods generally do not satisfy $I(q^{n+1}) = I(q^n)$. To address this, the entropy relaxation approach introduces a scalar entropy relaxation parameter, γ_n, modifying the solution update as

$$q(t_n + \gamma_n \Delta t) \approx q_{\gamma_n}^{n+1} = q^n + \gamma_n \Delta t \left(q^{n+1} - q^n\right),$$

with γ_n chosen to satisfy the nonlinear scalar equation

$$I\left(q_{\gamma_n}^{n+1}\right) = I(q^n).$$

Under certain mild conditions, $\gamma_n = 1 + \mathcal{O}(\Delta t^{p-1})$ exists and can be determined at each time step for a general nonlinear invariant I, where p is the order of the ImEx method [35, 45]. For specific invariants, such as energy represented by a solution norm, explicit formulas for γ_n are available [35, 45]. For an ImEx RK method with Butcher coefficients given in (14), the explicit formula for γ_n is given by

$$\gamma_n = \frac{-2\left\langle q^n,\ \Delta t \sum_{j=1}^s \left(\tilde{b}_j f_j + b_j g_j\right)\right\rangle}{\left\langle \Delta t \sum_{j=1}^s \left(\tilde{b}_j f_j + b_j g_j\right),\ \Delta t \sum_{j=1}^s \left(\tilde{b}_j f_j + b_j g_j\right)\right\rangle}, \tag{61}$$

where $f_j = f(q^{(j)})$ and $g_j = g(q^{(j)})$, are the function evaluations of f and g at the jth stage solution $q^{(j)}$. By constructing the entropy relaxation parameter, the modified solution preserves the invariant of the semidiscretized system, thereby ensuring the preservation of the invariant in the fully-discrete numerical scheme.

In the numerical experiments below, this entropy relaxation technique is used only where indicated in Sect. 4.2 and not at all in Sect. 4.1.

4 Numerical Experiments

In this section, we present the numerical results that validate the effectiveness and accuracy of the proposed methods for solving the KdVH system. We study solutions involving one or two solitons; a step-like initial condition leading to a dispersive shock wave has already been studied in [4]. We have implemented the numerical methods in Julia [5]. The spatial semidiscretizations and the Petviashvili method use SBP operators provided by the package SummationByPartsOperators.jl [44], wrapping FFTW [26] for Fourier methods. We use CairoMakie.jl [16] to visualize the results. The code to reproduce all numerical experiments is available in our reproducibility repository [8].

4.1 Numerical Tests of Asymptotic Preservation

We begin by comparing the solution of the KdV equation with those of the KdVH system for different values of τ. Specifically, we consider the KdV and the KdVH system on the domain $[x_L, x_R] \times (0, T] = [-40, 40] \times (0, 80]$ with periodic boundary conditions. We consider approximation of the soliton solution of the KdV equation:

$$\eta(x, t) = A \operatorname{sech}^2\left(\frac{\sqrt{3A}(x - ct)}{6}\right). \tag{62}$$

We use well-prepared initial data, meaning that we set $u(x, 0) = \eta(x, 0)$, $\boldsymbol{v}(0) = D_- \boldsymbol{\eta}(0)$ and $\boldsymbol{w}(0) = DD_- \boldsymbol{\eta}(0)$, where $D_\pm$ and D are upwind SBP derivative operators.

We discretize the spatial derivatives in both the KdV and KdVH equations using periodic FD SBP operators with $N = 2^8$ grid points. The semi-discrete system is integrated in time using the type II ARK method ARS(4,4,3) with a time step size of $\Delta t = 0.01$. With these fixed spatial and temporal parameters, Fig. 5 illustrates the convergence of the KdVH solution to that of the KdV equation as the relaxation parameter τ decreases.

To quantitatively validate the AP property of the schemes developed in Sect. 3.1, we examine the ℓ_2 norm induced by the mass/norm matrix M of the SBP operator used in space of the differences $\boldsymbol{u} - \boldsymbol{\eta}$, $\boldsymbol{v} - D_- \boldsymbol{\eta}$, and $\boldsymbol{w} - DD_- \boldsymbol{\eta}$, where $\boldsymbol{u}$, $\boldsymbol{v}$, and $\boldsymbol{w}$ represent the solutions of the fully discretized KdVH system, and $\boldsymbol{\eta}$ is a numerical solution of the KdV equation. For the numerical solutions of both the KdV and KdVH equations, we use spatial discretization based on periodic SBP operators on the domain $[-40, 40]$ with 2^{10} grid points. Below, we present the asymptotic errors for various ImEx time integrators, with four methods from each of type I and type II. In all cases, the time integrators use a fixed step size $\Delta t = 0.005$, and all errors are computed with respect to the numerical solution of the KdV equation at the final time $t = 16.67$.

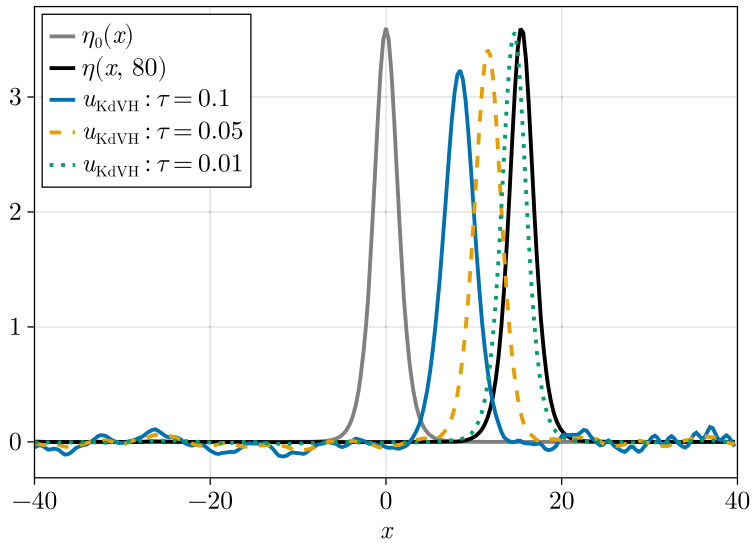

Fig. 5 Comparison of the solution of the KdV Eq. (1) (denoted by $\eta(x, 80)$) and its hyperbolic approximation (2) (denoted by '$u_{\mathrm{KdVH}} : \tau$') at time $t = 80$. In all cases, the solution is computed using a spatial discretization based on periodic SBP operators and the ARK method ARS(4,4,3) in time. The numerical solutions of the KdVH system converge to the numerical solution of the KdV equation as $\tau \to 0$

Table 1 Asymptotic errors and estimated orders of convergence (EOC) for the variables $\boldsymbol{u}$, $\boldsymbol{v}$, and $\boldsymbol{w}$ when integrating the KdVH system using the SSP2-ImEx(2,2,2) method

τ	$\|\|\boldsymbol{u} - \boldsymbol{\eta}\|\|_2$	EOC $\boldsymbol{u}$	$\|\|\boldsymbol{v} - D_-\boldsymbol{\eta}\|\|_2$	EOC $\boldsymbol{v}$	$\|\|\boldsymbol{w} - DD_-\boldsymbol{\eta}\|\|_2$	EOC $\boldsymbol{w}$
1.00e−01	3.77e+00		3.13e+00		3.61e+00	
1.00e−03	5.35e−02	0.92	4.47e−02	0.92	5.55e−02	0.91
1.00e−05	5.37e−04	1.00	8.96e−03	0.35	1.63e−02	0.27
1.00e−07	5.37e−06	1.00	9.51e−03	−0.01	1.69e−02	−0.01
1.00e−09	5.39e−08	1.00	9.52e−03	−0.00	1.69e−02	−0.00

The ℓ_2 norms of the errors are calculated relative to the numerical solution of the KdV equation, $\boldsymbol{\eta}$

4.1.1 AP Results for Type I ImEx-RK Methods

We begin with type I methods, denoted by NAME(s_E, s_I, p), where the triplet (s_E, s_I, p) specifies the number of stages in the explicit part (s_E), the number of stages in the implicit part (s_I), and the overall order (p) of the ImEx-RK method.

First, we consider a second-order type I method, denoted by SSP2-ImEx(2,2,2), as defined in Table 10. This method has an implicit part that is not SA and an explicit part that is not FSAL, meaning it is not GSA. However, the overall method is L-stable [9]. Table 1 presents the asymptotic errors in different variables. The scheme exhibits linear convergence of $\boldsymbol{u}$ as $\tau \to 0$, confirming the AP property for the $\boldsymbol{u}$-component, while for the variables $\boldsymbol{v}$ and $\boldsymbol{w}$, we do not observe the AP property of the method. This observation is in agreement with Theorem 1 and Remark 3, since this method does not have the GSA property.

We now examine another second-order type I method, SSP2-ImEx(3,3,2), as defined in Table 11. This method has an implicit part that is SA and an explicit part that does

Table 2 Asymptotic errors and estimated orders of convergence (EOC) for the variables $\boldsymbol{u}$, $\boldsymbol{v}$, and $\boldsymbol{w}$ when integrating the KdVH system using the SSP2-ImEx(3,3,2) method

τ	$\|\|\boldsymbol{u}-\boldsymbol{\eta}\|\|_2$	EOC $\boldsymbol{u}$	$\|\|\boldsymbol{v}-D_-\boldsymbol{\eta}\|\|_2$	EOC $\boldsymbol{v}$	$\|\|\boldsymbol{w}-DD_-\boldsymbol{\eta}\|\|_2$	EOC $\boldsymbol{w}$
1.00e−01	3.77e+00		3.13e+00		3.61e+00	
1.00e−03	5.35e−02	0.92	4.88e−02	0.90	6.31e−02	0.88
1.00e−05	5.36e−04	1.00	4.92e−04	1.00	6.46e−04	0.99
1.00e−07	5.36e−06	1.00	1.23e−05	0.80	2.61e−05	0.70
1.00e−09	5.38e−08	1.00	1.20e−05	0.01	2.62e−05	−0.00

The ℓ_2 norms of the errors are calculated relative to the numerical solution of the KdV equation, $\boldsymbol{\eta}$

Table 3 Asymptotic errors and estimated orders of convergence (EOC) for the variables $\boldsymbol{u}$, $\boldsymbol{v}$, and $\boldsymbol{w}$ when integrating the KdVH system using the AGSA(3,4,2) method

τ	$\|\|\boldsymbol{u}-\boldsymbol{\eta}\|\|_2$	EOC $\boldsymbol{u}$	$\|\|\boldsymbol{v}-D_-\boldsymbol{\eta}\|\|_2$	EOC $\boldsymbol{v}$	$\|\|\boldsymbol{w}-DD_-\boldsymbol{\eta}\|\|_2$	EOC $\boldsymbol{w}$
1.00e−01	3.80e+00		3.16e+00		3.63e+00	
1.00e−03	5.93e−02	0.90	5.44e−02	0.88	7.12e−02	0.85
1.00e−05	5.94e−04	1.00	5.50e−04	1.00	7.32e−04	0.99
1.00e−07	5.94e−06	1.00	5.49e−06	1.00	7.30e−06	1.00
1.00e−09	5.96e−08	1.00	7.93e−08	0.92	9.60e−08	0.94

The ℓ_2 norms of the errors are calculated relative to the numerical solution of the KdV equation, $\boldsymbol{\eta}$

not satisfy FSAL, which means it does not satisfy the GSA property. However, the overall method remains L-stable due to the SA property of the implicit part [9]. Table 2 shows the asymptotic errors for different variables. The convergence for the $\boldsymbol{u}$ variable demonstrates linear convergence as $\tau \to 0$, indicating the AP property for the $\boldsymbol{u}$-component. Additionally, compared to the SSP2-ImEx(2,2,2) method, the SSP2-ImEx(3,3,2) method shows improved convergence for the algebraic variables $\boldsymbol{v}$ and $\boldsymbol{w}$, despite both methods lacking the GSA property. We hypothesize that this improvement arises because the SSP2-ImEx(3,3,2) method only violates the FSAL property.

Now we consider a second-order type I method AGSA(3,4,2) given in Table 12 that satisfies the GSA property. Table 3 shows that we obtain AP properties for all the variables $\boldsymbol{u}$, $\boldsymbol{v}$, and $\boldsymbol{w}$, supporting our theoretical results for type I methods with the GSA property.

To test a high-order method of type I, we consider a third-order L-stable type I method SSP3-ImEx(3,4,3) given in Table 13, which is neither SA in the implicit part nor FSAL in the explicit part. Since this method does not possess the GSA property, we only expect the AP property in the $\boldsymbol{u}$-component, as shown in Table 4.

4.1.2 AP Results for Type II ImEx-RK Methods

In this section, we present the quantitative asymptotic errors for different type II methods. First, we consider a second-order ARS(2,2,2) method (in Table 14) and a third-order ARS(4,4,3) method (in Table 15), both of which are type II methods that satisfy the GSA property. We simulate the semi-discretized system with well-prepared initial data and present the asymptotic errors in Tables 5 and 6, respectively, for these two methods. The convergence rates in these tables illustrate the AP property for all the components with these two methods, as expected according to our theoretical results.

Table 4 Asymptotic errors and estimated orders of convergence (EOC) for the variables $\boldsymbol{u}$, $\boldsymbol{v}$, and $\boldsymbol{w}$ when integrating the KdVH system using the SSP3-ImEx(3,4,3) method

τ	$\|\|\boldsymbol{u}-\boldsymbol{\eta}\|\|_2$	EOC $\boldsymbol{u}$	$\|\|\boldsymbol{v}-D_-\boldsymbol{\eta}\|\|_2$	EOC $\boldsymbol{v}$	$\|\|\boldsymbol{w}-DD_-\boldsymbol{\eta}\|\|_2$	EOC $\boldsymbol{w}$
1.00e−01	3.77e+00		3.13e+00		3.60e+00	
1.00e−03	5.34e−02	0.92	4.88e−02	0.90	6.25e−02	0.88
1.00e−05	5.36e−04	1.00	3.73e−03	0.56	7.22e−03	0.47
1.00e−07	5.36e−06	1.00	3.82e−03	−0.01	6.80e−03	0.01
1.00e−09	5.38e−08	1.00	3.83e−03	−0.00	6.81e−03	−0.00

The ℓ_2 norms of the errors are calculated relative to the numerical solution of the KdV equation, $\boldsymbol{\eta}$

Table 5 Asymptotic errors and estimated orders of convergence (EOC) for the variables $\boldsymbol{u}$, $\boldsymbol{v}$, and $\boldsymbol{w}$ when integrating the KdVH system using the ARS(2,2,2) method

τ	$\|\|\boldsymbol{u}-\boldsymbol{\eta}\|\|_2$	EOC $\boldsymbol{u}$	$\|\|\boldsymbol{v}-D_-\boldsymbol{\eta}\|\|_2$	EOC $\boldsymbol{v}$	$\|\|\boldsymbol{w}-DD_-\boldsymbol{\eta}\|\|_2$	EOC $\boldsymbol{w}$
1.00e−01	3.77e+00		3.13e+00		3.61e+00	
1.00e−03	5.35e−02	0.92	4.88e−02	0.90	6.31e−02	0.88
1.00e−05	5.36e−04	1.00	4.89e−04	1.00	6.30e−04	1.00
1.00e−07	5.36e−06	1.00	4.89e−06	1.00	6.30e−06	1.00
1.00e−09	5.38e−08	1.00	5.01e−08	0.99	6.44e−08	1.00

The ℓ_2 norms of the errors are calculated relative to the numerical solution of the KdV equation, $\boldsymbol{\eta}$

Table 6 Asymptotic errors and estimated orders of convergence (EOC) for the variables $\boldsymbol{u}$, $\boldsymbol{v}$, and $\boldsymbol{w}$ when integrating the KdVH system using the ARS(4,4,3) method in time and an upwind FD method in space

τ	$\|\|\boldsymbol{u}-\boldsymbol{\eta}\|\|_2$	EOC $\boldsymbol{u}$	$\|\|\boldsymbol{v}-D_-\boldsymbol{\eta}\|\|_2$	EOC $\boldsymbol{v}$	$\|\|\boldsymbol{w}-DD_-\boldsymbol{\eta}\|\|_2$	EOC $\boldsymbol{w}$
1.00e−01	3.76e+00		3.13e+00		3.60e+00	
1.00e−03	5.34e−02	0.92	4.88e−02	0.90	6.31e−02	0.88
1.00e−05	5.36e−04	1.00	4.89e−04	1.00	6.31e−04	1.00
1.00e−07	5.36e−06	1.00	4.89e−06	1.00	6.31e−06	1.00
1.00e−09	5.38e−08	1.00	5.23e−08	0.99	6.50e−08	0.99

The ℓ_2 norms of the errors are calculated relative to the numerical solution of the KdV equation, $\boldsymbol{\eta}$

To demonstrate that the analysis of the properties is not limited to finite difference methods in space, we have also considered a DG method in space. The results for the ARS(4,4,3) method with a DG method using polynomials of degree 3 with 2^8 elements are presented in Table 7. We obtain similar results for Fourier pseudospectral methods, which are not shown here.

Tables 8 and 9 present the asymptotic errors for two methods: the third-order ARK3(2)4L[2]SA (in Table 16) and the fourth-order ARK4(3)6L[2]SA (in Table 17) of type II, as proposed by Kennedy and Carpenter [34]. Both methods do not have the GSA property, but their implicit parts are SA. The simulations are performed with well-prepared initial data, and the convergence rates shown in the tables indicate that we consistently obtain the AP property for the $\boldsymbol{u}$-component. It appears that we observe linear convergence rates for the algebraic variables within a certain range of τ values, as shown in the table, particularly for higher-order ImEx methods. This behavior surpasses the guarantees provided by the theoretical results for such methods. The observed effect is attributed to the use of a sufficiently

Table 7 Asymptotic errors and estimated orders of convergence (EOC) for the variables $\boldsymbol{u}$, $\boldsymbol{v}$, and $\boldsymbol{w}$ when integrating the KdVH system using the ARS(4,4,3) method in time and a DG method in space

τ	$\|\|\boldsymbol{u}-\boldsymbol{\eta}\|\|_2$	EOC $\boldsymbol{u}$	$\|\|\boldsymbol{v}-D_-\boldsymbol{\eta}\|\|_2$	EOC $\boldsymbol{v}$	$\|\|\boldsymbol{w}-DD_-\boldsymbol{\eta}\|\|_2$	EOC $\boldsymbol{w}$
1.00e−01	3.76e+00		3.13e+00		3.60e+00	
1.00e−03	5.34e−02	0.92	4.88e−02	0.90	6.31e−02	0.88
1.00e−05	5.36e−04	1.00	4.89e−04	1.00	6.31e−04	1.00
1.00e−07	5.36e−06	1.00	4.89e−06	1.00	6.31e−06	1.00
1.00e−09	5.36e−08	1.00	6.20e−08	0.95	6.39e−08	1.00

The ℓ_2 norms of the errors are calculated relative to the numerical solution of the KdV equation, $\boldsymbol{\eta}$

Table 8 Asymptotic errors and estimated orders of convergence (EOC) for the variables $\boldsymbol{u}$, $\boldsymbol{v}$, and $\boldsymbol{w}$ when integrating the KdVH system using the ARK3(2)4L[2]SA method

τ	$\|\|\boldsymbol{u}-\boldsymbol{\eta}\|\|_2$	EOC $\boldsymbol{u}$	$\|\|\boldsymbol{v}-D_-\boldsymbol{\eta}\|\|_2$	EOC $\boldsymbol{v}$	$\|\|\boldsymbol{w}-DD_-\boldsymbol{\eta}\|\|_2$	EOC $\boldsymbol{w}$
1.00e−01	3.77e+00		3.13e+00		3.60e+00	
1.00e−03	5.34e−02	0.92	4.88e−02	0.90	6.32e−02	0.88
1.00e−05	5.36e−04	1.00	4.90e−04	1.00	6.37e−04	1.00
1.00e−07	5.36e−06	1.00	1.27e−05	0.79	2.69e−05	0.69
1.00e−09	5.38e−08	1.00	1.24e−05	0.01	2.71e−05	−0.00

The ℓ_2 norms of the errors are calculated relative to the numerical solution of the KdV equation, $\boldsymbol{\eta}$

Table 9 Asymptotic errors and estimated orders of convergence (EOC) for the variables $\boldsymbol{u}$, $\boldsymbol{v}$, and $\boldsymbol{w}$ when integrating the KdVH system using the ARK4(3)6L[2]SA method. The ℓ_2 norms of the errors are calculated relative to the numerical solution of the KdV equation, $\boldsymbol{\eta}$

τ	$\|\|\boldsymbol{u}-\boldsymbol{\eta}\|\|_2$	EOC $\boldsymbol{u}$	$\|\|\boldsymbol{v}-D_-\boldsymbol{\eta}\|\|_2$	EOC $\boldsymbol{v}$	$\|\|\boldsymbol{w}-DD_-\boldsymbol{\eta}\|\|_2$	EOC $\boldsymbol{w}$
1.00e−01	3.77e+00		3.13e+00		3.60e+00	
1.00e−03	5.34e−02	0.92	4.88e−02	0.90	6.31e−02	0.88
1.00e−05	5.36e−04	1.00	4.89e−04	1.00	6.31e−04	1.00
1.00e−07	5.36e−06	1.00	4.89e−06	1.00	6.31e−06	1.00
1.00e−09	5.38e−08	1.00	4.97e−08	1.00	6.35e−08	1.00

The ℓ_2 norms of the errors are calculated relative to the numerical solution of the KdV equation, $\boldsymbol{\eta}$

small time step in the simulation. However, with a larger time step, we observe that the AP property manifests only in the $\boldsymbol{u}$-component, not in the algebraic variables.

4.1.3 Asymptotic-Accuracy Property

The various classes of ImEx methods employed in the numerical experiments presented here have been proven to satisfy the AP and AA properties for hyperbolic relaxation systems, as established in [42]. Analogous results hold for the relaxation system considered in this study, as demonstrated in Sect. 3.1. In this section, we numerically investigate the AA property for different classes of ImEx methods with two values of the relaxation parameter, capturing distinct regimes of the relaxation limit. Specifically, we select $\tau \in \{10^{-5}, 10^{-9}\}$ and demonstrate error convergence for each τ using five methods: AGSA(3,4,2), SSP3-ImEx(3,4,3), ARS(2,2,2), ARS(4,4,3), and ARK3(2)4L[2]SA.

For all experiments, we use an 8th-order periodic first-derivative upwind SBP operator with $N = 2^{10}$ spatial grid points on the domain $[-40, 40]$ for spatial semi-discretization. The error convergence for the components $\boldsymbol{u}$, $\boldsymbol{v}$, and $\boldsymbol{w}$ at $t = 4.8$ is illustrated in Fig. 6. The error at the final time is computed relative to reference solutions of the KdVH system denoted by $\boldsymbol{u_P}$, $\boldsymbol{v_P}$, and $\boldsymbol{w_P}$, where $\boldsymbol{u_P}$ is obtained using a Petviashvili-type method on a fine spatial grid with 2^{11} grid points. The reference solution for the auxiliary variable $\boldsymbol{w_P} = c\boldsymbol{u_P} - \frac{\boldsymbol{u_P}^2}{2}$ is derived by integrating (5a), and $\boldsymbol{v_P} = D_-\boldsymbol{u_P} - c\tau D_-\boldsymbol{w_P}$ is obtained by using (5c).

In accordance with our theoretical results, the methods AGSA(3,4,2), ARS(2,2,2) and ARS(4,4,3) confirm the AA property for all components. The method SSP3-ImEx(3,4,3) exhibits the AA property for the $\boldsymbol{u}$-component only but not for the auxiliary components, aligning with theoretical predictions. Additionally, we observe the AA property for the $\boldsymbol{u}$-component with the ARK3(2)4L[2]SA method, despite this property not being theoretically guaranteed for this method, a behavior similar to its AP property.

4.2 Numerical Tests of Energy Conservation

It is well-known that integrating the KdV equation with an energy-conserving numerical scheme results in linear error growth over time, whereas a non-conservative method leads to quadratic error growth [17]. This distinction makes conservative methods superior for maintaining solution accuracy over long time intervals. The KdVH system has a modified energy that is conserved, and as the relaxation parameter $\tau \to 0$, this energy converges to that of the KdV equation. We aim to examine the effect of numerically conserving this modified energy on error propagation in the KdVH system across different values of τ. To achieve this, we use an energy-conserving spatial semi-discretization combined with a relaxation Runge–Kutta approach, specifically designed to preserve one or more invariants of the system. For error computation in the KdVH system, we use the analytical solution (or a highly accurate numerical solution) of the KdV equation as the reference.

Considering the spatial domain $[-40, 40]$ with 2^8 grid points and an 8th-order finite-difference operator for derivatives, we integrate the energy-conserving semi-discretized KdVH system up to a final time of 333.34 using the ARK method ARS(4,4,3), with and without entropy relaxation. In each case we start the time stepping with a fixed time step $\Delta t = 0.05$. Errors at each time step are computed with respect to the analytical solution of the KdV equation, and Fig. 7 presents the error growth profiles for four values of τ. Each panel in the figure includes reference error growth curves for the KdV equation, demonstrating linear versus quadratic error growth for conservative versus non-conservative methods. For smaller τ values, we observe similar behavior in error growth for the KdVH system, while for larger τ values, this behavior becomes less evident. Expected linear and quadratic error growth behaviors for conservative and non-conservative methods, respectively, are observed only when τ is sufficiently small. Additionally, as τ decreases, the error growth curves for the KdVH system converge toward those of the KdV system.

To examine the effects of energy conservation using different ImEx integrators for the KdVH system with different values of the relaxation parameter τ with a more challenging solution, we consider the KdV equation and the hyperbolized system with a 2-soliton solution given by

$$u(x,t) = -\frac{12(\beta_1 - \beta_2)\left(\beta_2 \operatorname{csch}^2(\xi_2) + \beta_1 \operatorname{sech}^2(\xi_1)\right)}{\left(\sqrt{2\beta_1}\tanh(\xi_1) - \sqrt{2\beta_2}\coth(\xi_2)\right)^2}\,. \tag{63}$$

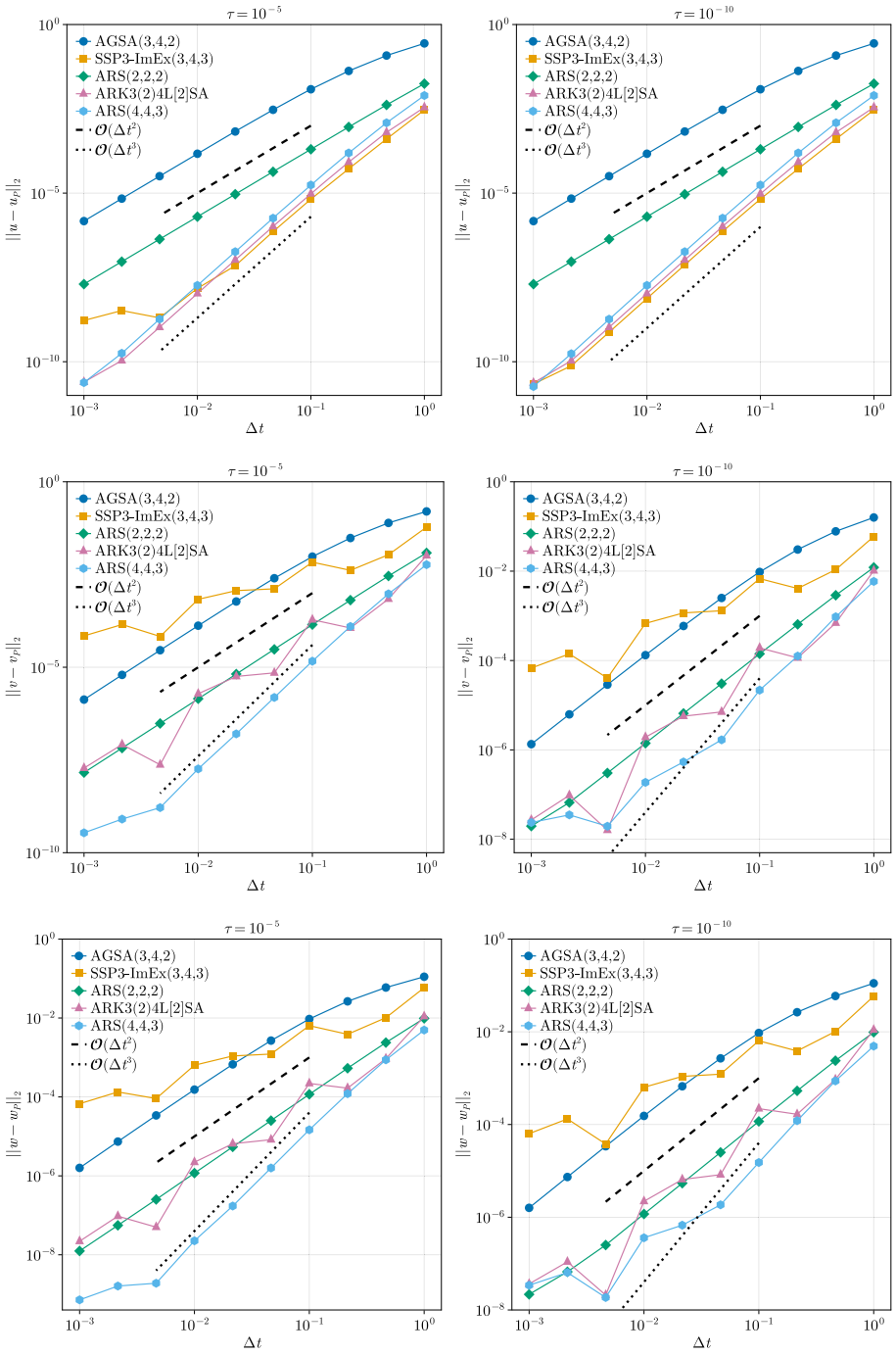

Fig. 6 Error convergence for variables $\boldsymbol{u}$ (top row), $\boldsymbol{v}$ (middle row), and $\boldsymbol{w}$ (bottom row) for two relaxation parameters. The reference solutions $\boldsymbol{u_P}$, $\boldsymbol{v_P}$, and $\boldsymbol{w_P}$ are obtained using a Petviashvili-type method and a periodic first-derivative SBP operator. The methods AGSA(3,4,2), SSP3-ImEx(3,4,3), ARS(2,2,2), and ARS(4,4,3) exhibit the expected AA property for all components, whereas ARK3(2)4L[2]SA demonstrates the AA property for the $\boldsymbol{u}$-component, which is beyond our guaranteed theoretical results

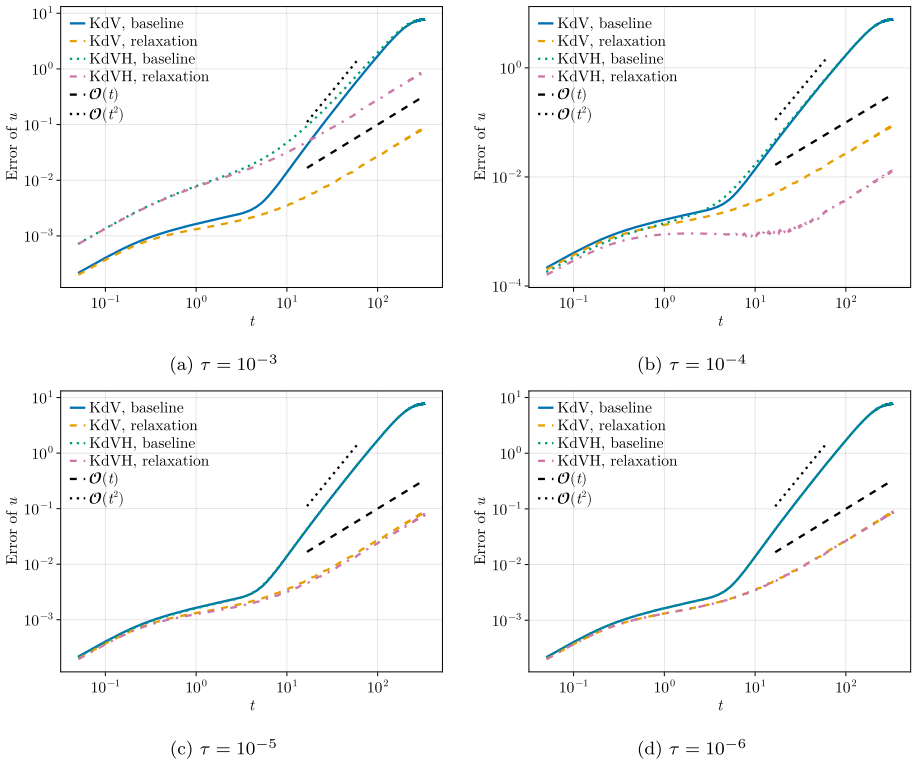

Fig. 7 Error growth profiles for the KdVH system up to time $t = 333.34$ for four values of the relaxation parameter τ. Each subplot compares the numerical solutions with the analytical solitary wave solution of the KdV equation. For smaller τ, linear error growth characteristic of conservative methods is observed. As τ decreases, the error growth curves for the KdVH system converge towards those of the KdV system

where $\beta_1 = 0.5$, $\beta_2 = 1$, $\xi_1 = \frac{\sqrt{\beta_1}(x-2\beta_1 t)}{\sqrt{2}}$, and $\xi_2 = \frac{\sqrt{\beta_2}(x-2\beta_2 t)}{\sqrt{2}}$. In this case, we consider the domain $[-60, 100]$ with 2^{10} grid points and employ an 8th-order energy-conserving finite-difference operator for spatial semidiscretization. We integrate the energy-conserving semidiscretized systems for both the KdV equation and the KdVH system with $\tau = 10^{-3}$ and $\tau = 10^{-5}$ from $t = -20$ to $t = 50$ using different time-stepping methods, both with and without entropy relaxation. We initialize the simulation from a negative time to capture the soliton interaction occurring at $t = 0$. Consequently, when plotting error growth over time on a log-log scale, the time axis is shifted by the starting time. For time integration, we use AGSA(3,4,2), ARS(4,4,3), and ARK4(3)6L[2]SA, with initial time steps $\Delta t = 0.02, 0.1$, and 0.5, respectively.

Figure 8 presents the error growth profiles for the three methods with two values of τ. At each time step, the error is computed relative to the analytical 2-soliton solution given by (63). For each method, the time-stepping approach with entropy relaxation exhibits improved error growth compared to its corresponding baseline method. Notably, all methods display a dip in the error growth profile during soliton interaction, consistent with previous observations [7, 17]. Furthermore, as τ decreases, the error growth curves progressively converge toward those of the KdV system.

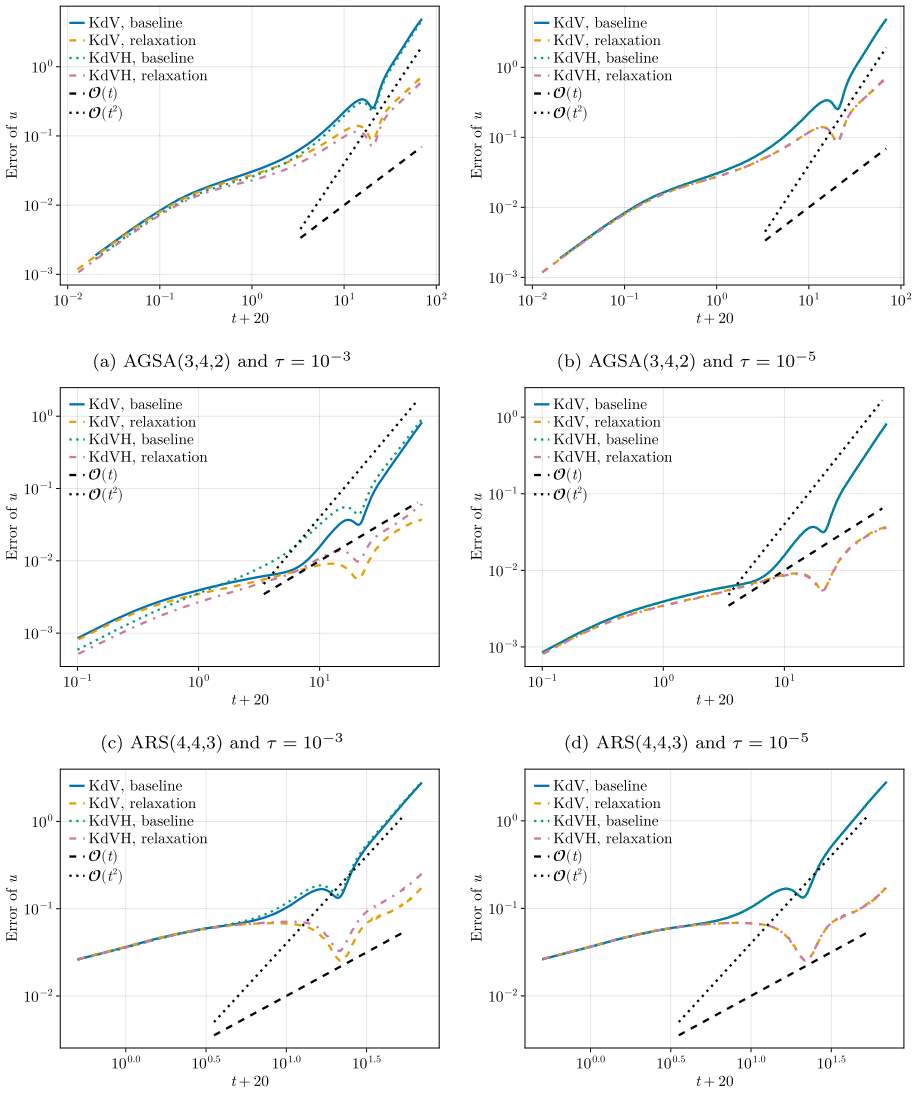

(a) AGSA(3,4,2) and $\tau = 10^{-3}$

(b) AGSA(3,4,2) and $\tau = 10^{-5}$

(c) ARS(4,4,3) and $\tau = 10^{-3}$

(d) ARS(4,4,3) and $\tau = 10^{-5}$

(e) ARK4(3)6L[2]SA and $\tau = 10^{-3}$

(f) ARK4(3)6L[2]SA and $\tau = 10^{-5}$

Fig. 8 Error growth profiles for the KdVH system with two values of the relaxation parameter τ, computed from $t = -20$ to $t = 50$ using three different ImEx methods. Each subplot compares the numerical solutions with the analytical 2-soliton solution of the KdV equation. ImEx methods with entropy relaxation exhibit improved error growth compared to their corresponding baseline methods. Furthermore, as τ decreases, the error growth curves for the KdVH system converge toward those of the KdV system

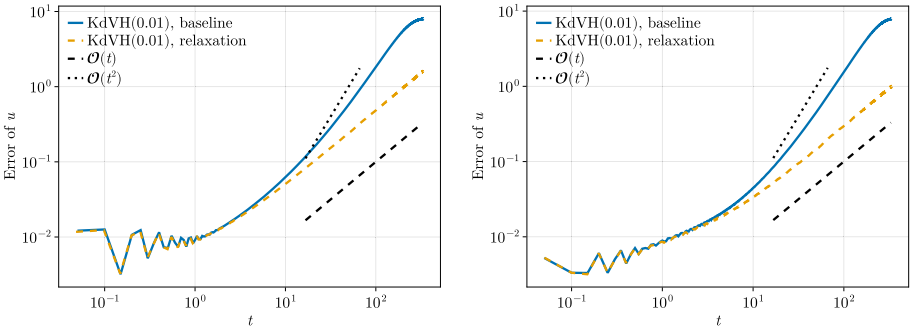

(a) Error growth by SSP2-IMEX(2,2,2)

(b) Error growth by ARS(2,2,2)

Fig. 9 Error growth profiles for the KdVH system with $\tau = 10^{-2}$ up to time $t = 333.34$. The left panel shows the error growth by SSP2-IMEX(2,2,2) with and without entropy relaxation, while the right panel shows the error growth by ARS(2,2,2). In each case, the numerical solution is compared with the numerically obtained exact solution of the KdVH system

So far, we have examined the error growth over time by measuring the solution error of the KdVH system with respect to the analytical solution of the KdV equation. Now, given a particular value of τ, we focus on the KdVH system itself and compare its numerical solution with the numerically obtained exact solution of the KdVH system, computed using the Petviashvili method. The Petviashvili method is applied over the domain $[-40, 40]$ with 2^{10} grid points to obtain numerically exact solitary wave solutions for the KdVH system with $\tau = 10^{-2}$. For the numerical solution, we semi-discretize the KdVH using an 8th-order upwind finite difference approximation with 2^8 grid points, resulting in a modified energy-preserving semidiscretization. Figure 9 shows the error growth for two different ImEx-RK methods: SSP2-IMEX(2,2,2), a type I method, and ARS(2,2,2), a type II method. All time integrations are initialized with a time step of $\Delta t = 0.05$. Both methods exhibit the expected linear and quadratic error growth over time when integrated with and without entropy relaxation.

5 Conclusions

Given the increasing interest in hyperbolic approximations to dispersive nonlinear wave equations, it is of great interest to understand the dynamics of these hyperbolic models and develop structure-preserving numerical discretizations for them. Here we have carried out this work in relation to the hyperbolized KdV system.

One of our principal findings is that the dynamics of the KdVH system, studied here primarily in terms of traveling waves, is in a sense richer than that of the original KdV equation, and includes additional classes of solitary and periodic waves including some with lower regularity. A more extensive investigation of these solutions, along the lines of [37], would be very interesting. Furthermore, the resemblance of (11) and its solutions to higher-order water wave models suggests that there may be a deeper connection between KdVH and such models.

The asymptotic-preserving discretizations developed herein provide essential guarantees for numerical solutions of KdVH, since in practice one uses a finite value of the relaxation parameter τ. Numerical results of asymptotic preservation and asymptotic accuracy presented

herein support our theoretical results, with some ImEx methods by Kennedy and Carpenter of type II [34] producing results that outperform theoretical predictions, suggesting the need for further investigation to fully understand this behavior. Energy preservation ensures that solutions of KdVH remain closer to those of KdV for longer times. It would be of interest to investigate the existence of higher-order modified invariants of KdVH and their numerical preservation.

Appendix

A Type I ImEx methods

A.1 SSP2-ImEx(2,2,2)

Table 10 Tableau for the 2nd-order L-stable type I ImEx-RK method: the explicit part is not FSAL, the implicit part is not SA, hence not GSA, with $\gamma = 1 - \frac{1}{\sqrt{2}}$

0	0	0	γ	γ	0
1	1	0	$1-\gamma$	$1-2\gamma$	γ
	1/2	1/2		1/2	1/2

A.2 SSP2-ImEx(3,3,2)

Table 11 Tableau for the 2nd-order L-stable type I ImEx-RK method: the explicit part is not FSAL, the implicit part is SA, hence not GSA

0	0	0	0	1/4	1/4	0	0
1/2	1/2	0	0	1/4	0	1/4	0
1	1/2	1/2	0	1	1/3	1/3	1/3
	1/3	1/3	1/3		1/3	1/3	1/3

A.3 AGSA(3,4,2)

Table 12 Tableau for the 2nd-order type I ImEx-RK method: the explicit part is FSAL, the implicit part is SA, hence GSA

0	0	0	0	0	c_1	c_1	0	0	0
$\tilde{c}_2$	$\tilde{c}_2$	0	0	0	c_2	a_{21}	a_{22}	0	0
$\tilde{c}_3$	$\tilde{a}_{31}$	$\tilde{a}_{32}$	0	0	c_3	a_{31}	a_{32}	a_{33}	0
1	$\tilde{b}_1$	$\tilde{b}_2$	$\tilde{b}_3$	0	1	b_1	b_2	b_3	γ
	$\tilde{b}_1$	$\tilde{b}_2$	$\tilde{b}_3$	0		b_1	b_2	b_3	γ

The coefficients in the table are $c_2 = \tilde{a}_{21} = \frac{-139833537}{38613965}$, $c_1 = \frac{168999711}{74248304}$, $\tilde{a}_{31} = \frac{85870407}{49798258}$, $\gamma = a_{22} = \frac{202439144}{118586105}$, $\tilde{a}_{32} = \frac{-121251843}{1756367063}$, $a_{33} = \frac{12015439}{183058594}$, $\tilde{b}_2 = \frac{1}{6}$, $\tilde{b}_3 = \frac{2}{3}$, $a_{31} = \frac{-6418119}{169001713}$, $a_{21} = \frac{44004295}{24775207}$, $\tilde{a}_{32} = \frac{-748951821}{1043823139}$, $b_2 = \frac{1}{3}$, $b_3 = 0$, $\tilde{b}_1 = 1-\tilde{b}_2-\tilde{b}_3$, and $b_1 = 1-\gamma-b_2-b_3$.

A.4 SSP3-ImEx(3,4,3)

Table 13 Tableau for the 3rd-order L-stable type I ImEx-RK method: the explicit part is not FSAL, the implicit part is not SA, hence not GSA

0	0	0	0	0	α	α	0	0	0
0	0	0	0	0	0	$-\alpha$	α	0	0
1	0	1	0	0	1	0	$1-\alpha$	α	0
1/2	0	1/4	1/4	0	1/2	β	η	$1/2-\beta-\eta-\alpha$	α
	0	1/6	1/6	2/3		0	1/6	1/6	2/3

where $\alpha = 0.241694260788$, $\beta = 0.0604235651970$, and $\eta = 0.12915286960590$.

B Type II ImEx methods

B.1 ARS(2,2,2)

Table 14 Tableau for the ARS(2,2,2) method: the explicit part is FSAL, the implicit part is SA, hence GSA, with coefficients $\gamma = 1 - \frac{1}{\sqrt{2}}$ and $\delta = 1 - \frac{1}{2\gamma}$

0	0	0	0	0	0	0	0
γ	γ	0	0	γ	0	γ	0
1	δ	$1-\delta$	0	1	0	$1-\gamma$	γ
	δ	$1-\delta$	0		0	$1-\gamma$	γ

B.2 ARS(4,4,3)

Table 15 Tableau for the ARS(4,4,3) method: the explicit part is FSAL, the implicit part is SA, hence GSA

0	0	0	0	0	0	0	0	0	0	0	0
1/2	1/2	0	0	0	0	1/2	0	1/2	0	0	0
2/3	11/18	1/18	0	0	0	2/3	0	1/6	1/2	0	0
1/2	5/6	−5/6	1/2	0	0	1/2	0	−1/2	1/2	1/2	0
1	1/4	7/4	3/4	−7/4	0	1	0	3/2	−3/2	1/2	1/2
	1/4	7/4	3/4	−7/4	0		0	3/2	−3/2	1/2	1/2

B.3 ARK3(2)4 L[2]SA

Table 16 Tableau for the ARK3(2)4 L[2]SA method: the explicit part is not FSAL, the implicit part is SA, hence not GSA

0	0	0	0	0	0	0	0	0	0
$\frac{1767732205903}{2027836641118}$	$\frac{1767732205903}{2027836641118}$	0	0	0	$\frac{1767732205903}{2027836641118}$	$\frac{1767732205903}{4055673282236}$	$\frac{1767732205903}{4055673282236}$	0	0
$\frac{3}{5}$	$\frac{5535828885825}{10492691773637}$	$\frac{788022342437}{10882634858940}$	0	0	$\frac{3}{5}$	$\frac{2746238789719}{10658868560708}$	$\frac{-640167445237}{6845629431997}$	$\frac{1767732205903}{4055673282236}$	0
1	$\frac{6485989280629}{16251701735622}$	$\frac{-4246266847089}{9704473918619}$	$\frac{10755448449292}{10357097424841}$	0	1	$\frac{1471266399579}{7840856788654}$	$\frac{-4482444167858}{7529755066697}$	$\frac{11266239266428}{11593286722821}$	$\frac{1767732205903}{4055673282236}$
	$\frac{1471266399579}{7840856788654}$	$\frac{-4482444167858}{7529755066697}$	$\frac{11266239266428}{11593286722821}$	$\frac{1767732205903}{4055673282236}$		$\frac{1471266399579}{7840856788654}$	$\frac{-4482444167858}{7529755066697}$	$\frac{11266239266428}{11593286722821}$	$\frac{1767732205903}{4055673282236}$

B.4 ARK4(3)6 L[2]SA

Table 17 Tableau for the ARK4(3)6L[2]SA method: the explicit part is not FSAL, the implicit part is SA, hence not GSA

0	0	0	0	0	0	0	0	0	0	0	0	0	0
$\frac{1}{2}$	$\frac{1}{2}$	0	0	0	0	0	$\frac{1}{2}$	$\frac{1}{4}$	$\frac{1}{4}$	0	0	0	0
$\frac{83}{250}$	$\frac{13861}{62500}$	$\frac{6889}{62500}$	0	0	0	0	$\frac{83}{250}$	$\frac{8611}{62500}$	$\frac{-1743}{31250}$	$\frac{1}{4}$	0	0	0
$\frac{31}{50}$	$\frac{-116923316275}{2393684061468}$	$\frac{-2731218467317}{15368042101831}$	$\frac{9408046702089}{11113171139209}$	0	0	0	$\frac{31}{50}$	$\frac{5012029}{34652500}$	$\frac{-654441}{2922500}$	$\frac{174375}{388108}$	$\frac{1}{4}$	0	0
$\frac{17}{20}$	$\frac{-451086348788}{2902428689909}$	$\frac{-2682348792572}{7519795681897}$	$\frac{12662868775082}{11960479115383}$	$\frac{3355817975965}{11060851509271}$	0	0	$\frac{17}{20}$	$\frac{15267082809}{155376265600}$	$\frac{-71443401}{120774400}$	$\frac{730878875}{902184768}$	$\frac{2285395}{8070912}$	$\frac{1}{4}$	0
1	$\frac{647845179188}{3216320057751}$	$\frac{73281519250}{8382639484533}$	$\frac{552539513391}{3454668386233}$	$\frac{3354512671639}{8306763924573}$	$\frac{4040}{17871}$	0	1	$\frac{82889}{524892}$	0	$\frac{15625}{83664}$	$\frac{69875}{102672}$	$\frac{-2260}{8211}$	$\frac{1}{4}$
	$\frac{82889}{524892}$	0	$\frac{15625}{83664}$	$\frac{69875}{102672}$	$\frac{-2260}{8211}$	$\frac{1}{4}$		$\frac{82889}{524892}$	0	$\frac{15625}{83664}$	$\frac{69875}{102672}$	$\frac{-2260}{8211}$	$\frac{1}{4}$

Funding Open access publishing provided by King Abdullah University of Science and Technology (KAUST). AB and DK were supported by the King Abdullah University of Science and Technology (KAUST). HR was supported by the Deutsche Forschungsgemeinschaft (DFG, German Research Foundation, project number 513301895) and the Daimler und Benz Stiftung (Daimler and Benz foundation, project number 32-10/22).

Data Availability The datasets and source code generated and analyzed during the current study are available in [8].

Declarations

Conflict of interest On behalf of all authors, the corresponding author declares that they have no conflict of interest.

References

1. Álvarez, J., Durán, A.: Petviashvili type methods for traveling wave computations: I. Analysis of convergence. J. Comput. Appl. Math. **266**, 39–51 (2014)
2. Antuono, M., Liapidevskii, V., Brocchini, M.: Dispersive nonlinear shallow-water equations. Stud. Appl. Math. **122**(1), 1–28 (2009)
3. Bassi, C., Bonaventura, L., Busto, S., Dumbser, M.: A hyperbolic reformulation of the Serre-Green-Naghdi model for general bottom topographies. Comput. Fluids **212**, 104716 (2020)
4. Besse, C., Gavrilyuk, S., Kazakova, M., Noble, P.: Perfectly matched layers methods for mixed hyperbolic-dispersive equations. Water Waves **4**(3), 313–343 (2022)
5. Bezanson, J., Edelman, A., Karpinski, S., Shah, V.B.: Julia: a fresh approach to numerical computing. SIAM Rev. **59**(1), 65–98 (2017). https://doi.org/10.1137/141000671
6. Biswas, A., Ketcheson, D.I.: Accurate solution of the nonlinear Schrödinger equation via conservative multiple-relaxation ImEx methods. SIAM J. Sci. Comput. **46**(6), A3827–A3848 (2024). https://doi.org/10.1137/23M1598118
7. Biswas, A., Ketcheson, D.I.: Multiple-relaxation Runge Kutta methods for conservative dynamical systems. J. Sci. Comput. **97**(1), 4 (2023)
8. Biswas, A., Ketcheson, D.I., Ranocha, H., Schütz, J.: Reproducibility repository for "Traveling-wave solutions and structure-preserving numerical methods for a hyperbolic approximation of the Korteweg-de Vries equation". https://github.com/abhibsws/2024_kdvh_RR (2024). https://doi.org/10.5281/zenodo.14423351
9. Boscarino, S., Russo, G.: Asymptotic preserving methods for quasilinear hyperbolic systems with stiff relaxation: a review. SeMA J. **81**(1), 3–49 (2024)
10. Brun, M.K., Kalisch, H.: Convective wave breaking in the KdV equation. Anal. Math. Phys. **8**, 57–75 (2018)
11. Camassa, R., Holm, D.D., Hyman, J.M.: A new integrable shallow water equation. Adv. Appl. Mech. **31**, 1–33 (1994)
12. Chesnokov, A., Ermishina, V., Liapidevskii, V.Y.: Strongly non-linear Boussinesq-type model of the dynamics of internal solitary waves propagating in a multilayer stratified fluid. Phys. Fluids **35**(7), 076605 (2023)
13. Chesnokov, A., Nguyen, T.H.: Hyperbolic model for free surface shallow water flows with effects of dispersion, vorticity and topography. Comput. Fluids **189**, 13–23 (2019)
14. Constantin, A.: Finite propagation speed for the Camassa-Holm equation. J. Math. Phys. **46**(2), 023506 (2005)

15. Constantin, A., Lannes, D.: The hydrodynamical relevance of the Camassa-Holm and Degasperis-Procesi equations. Arch. Ration. Mech. Anal. **192**, 165–186 (2009)
16. Danisch, S., Krumbiegel, J.: Makie.jl: flexible high-performance data visualization for Julia. J. Open Source Softw. **6**(65), 3349 (2021). https://doi.org/10.21105/joss.03349
17. De Frutos, J., Sanz-Serna, J.M.: Accuracy and conservation properties in numerical integration: the case of the Korteweg-de Vries equation. Numer. Math. **75**(4), 421–445 (1997). https://doi.org/10.1007/s002110050247
18. Dhaouadi, F., Dumbser, M.: A first order hyperbolic reformulation of the Navier-Stokes-Korteweg system based on the GPR model and an augmented Lagrangian approach. J. Comput. Phys. **470**, 111544 (2022)
19. Dhaouadi, F., Favrie, N., Gavrilyuk, S.: Extended Lagrangian approach for the defocusing nonlinear Schrödinger equation. Stud. Appl. Math. **142**(3), 336–358 (2019)
20. Dhaouadi, F., Gavrilyuk, S., Vila, J.P.: Hyperbolic relaxation models for thin films down an inclined plane. Appl. Math. Comput. **433**, 127378 (2022)
21. Durán, A., Sanz-Serna, J.M.: The numerical integration of relative equilibrium solutions. Geometric theory. Nonlinearity **11**(6), 1547 (1998). https://doi.org/10.1088/0951-7715/11/6/008
22. Durán, A., Sanz-Serna, J.M.: The numerical integration of relative equilibrium solutions. The nonlinear Schrödinger equation. IMA J. Numer. Anal. **20**(2), 235–261 (2000). https://doi.org/10.1093/imanum/20.2.235
23. Escalante, C., Dumbser, M., Castro, M.J.: An efficient hyperbolic relaxation system for dispersive non-hydrostatic water waves and its solution with high order discontinuous Galerkin schemes. J. Comput. Phys. **394**, 385–416 (2019)
24. Favrie, N., Gavrilyuk, S.: A rapid numerical method for solving Serre-Green-Naghdi equations describing long free surface gravity waves. Nonlinearity **30**(7), 2718 (2017)
25. Fernández, D.C.D.R., Hicken, J.E., Zingg, D.W.: Review of summation-by-parts operators with simultaneous approximation terms for the numerical solution of partial differential equations. Comput. Fluids **95**, 171–196 (2014). https://doi.org/10.1016/j.compfluid.2014.02.016
26. Frigo, M., Johnson, S.G.: The design and implementation of FFTW3. Proc. IEEE **93**(2), 216–231 (2005). https://doi.org/10.1109/JPROC.2004.840301
27. Gavrilyuk, S., Nkonga, B., Shyue, K.M.: The conduit equation: Hyperbolic approximation and generalized Riemann problem. Available at SSRN 4724161 (2024)
28. Gavrilyuk, S., Shyue, K.M.: Hyperbolic approximation of the BBM equation. Nonlinearity **35**(3), 1447 (2022)
29. Grosso, G., Antuono, M., Brocchini, M.: Dispersive nonlinear shallow-water equations: some preliminary numerical results. J. Eng. Math. **67**, 71–84 (2010)
30. Harris, C.R., Millman, K.J., Van Der Walt, S.J., Gommers, R., Virtanen, P., Cournapeau, D., Wieser, E., Taylor, J., Berg, S., Smith, N.J., Kern, R., Picus, M., Hoyer, S., van Kerkwijk, M.H., Brett, M., Haldane, A., Del Río, J.F., Wiebe, M., Peterson, P., Gérard-Marchant, P., Sheppard, K., Reddy, T., Weckesser, W., Abbasi, H., Gohlke, C., Oliphant, T.E.: Array programming with NumPy. Nature **585**(7825), 357–362 (2020). https://doi.org/10.1038/s41586-020-2649-2
31. Hunter, J.D.: Matplotlib: a 2D graphics environment. Comput. Sci. Eng. **9**(3), 90–95 (2007). https://doi.org/10.1109/MCSE.2007.55
32. Jin, S.: Asymptotic preserving (AP) schemes for multiscale kinetic and hyperbolic equations: a review. Riv. Mat. Della Univ. Parma **3**, 177–216 (2012)
33. Jin, S.: Asymptotic-preserving schemes for multiscale physical problems. Acta Numer. **31**, 415–489 (2022). https://doi.org/10.1017/S0962492922000010
34. Kennedy, C.A., Carpenter, M.H.: Additive Runge-Kutta schemes for convection-diffusion-reaction equations. Appl. Numer. Math. **44**(1–2), 139–181 (2003)
35. Ketcheson, D.I.: Relaxation Runge-Kutta methods: conservation and stability for inner-product norms. SIAM J. Numer. Anal. **57**(6), 2850–2870 (2019)
36. Ketcheson, D.I., Biswas, A.: Approximation of arbitrarily high-order pdes by first-order hyperbolic relaxation. Nonlinearity **38**(5), 055002 (2025). https://doi.org/10.1088/1361-6544/adc6e8
37. Lenells, J.: Traveling wave solutions of the Degasperis-Procesi equation. J. Math. Anal. Appl. **306**(1), 72–82 (2005)
38. Li, D., Li, X., Zhang, Z.: Implicit-explicit relaxation Runge-Kutta methods: construction, analysis and applications to PDEs. Math. Comput. (2022). https://doi.org/10.1090/mcom/3766
39. Li, L., Lou, J., Luo, H., Nishikawa, H.: A new formulation of hyperbolic Navier-Stokes solver based on finite volume method on arbitrary grids. In: 2018 Fluid Dynamics Conference, p. 4160 (2018)
40. Mattsson, K.: Diagonal-norm upwind SBP operators. J. Comput. Phys. **335**, 283–310 (2017). https://doi.org/10.1016/j.jcp.2017.01.042

41. Mazaheri, A., Ricchiuto, M., Nishikawa, H.: A first-order hyperbolic system approach for dispersion. J. Comput. Phys. **321**(Supplement C), 593–605 (2016)
42. Pareschi, L., Russo, G.: Implicit-explicit Runge-Kutta schemes and applications to hyperbolic systems with relaxation. J. Sci. Comput. **25**, 129–155 (2005)
43. Ranocha, H.: Mimetic properties of difference operators: product and chain rules as for functions of bounded variation and entropy stability of second derivatives. BIT Numer. Math. **59**(2), 547–563 (2019). https://doi.org/10.1007/s10543-018-0736-7
44. Ranocha, H.: SummationByPartsOperators.jl: a Julia library of provably stable semidiscretization techniques with mimetic properties. J. Open Source Softw. **6**(64), 3454 (2021). https://doi.org/10.21105/joss.03454
45. Ranocha, H., Lóczi, L., Ketcheson, D.I.: General relaxation methods for initial-value problems with application to multistep schemes. Numer. Math. **146**, 875–906 (2020). https://doi.org/10.1007/s00211-020-01158-4
46. Ranocha, H., Mitsotakis, D., Ketcheson, D.I.: A broad class of conservative numerical methods for dispersive wave equations. Commun. Comput. Phys. **29**(4), 979–1029 (2021). https://doi.org/10.4208/cicp.OA-2020-0119
47. Ranocha, H., Sayyari, M., Dalcin, L., Parsani, M., Ketcheson, D.I.: Relaxation Runge-Kutta methods: fully-discrete explicit entropy-stable schemes for the compressible Euler and Navier-Stokes equations. SIAM J. Sci. Comput. **42**(2), A612–A638 (2020). https://doi.org/10.1137/19M1263480
48. Richtmyer, R.D., Morton, K.W.: Difference Methods for Boundary-Value Problems. Wiley, New York, London, Sydney (1967)
49. Rüter, H.R., Hilditch, D., Bugner, M., Brügmann, B.: Hyperbolic relaxation method for elliptic equations. Phys. Rev. D **98**(8), 084044 (2018)
50. Schütz, J., Noelle, S.: Flux splitting for stiff equations: a notion on stability. J. Sci. Comput. **64**(2), 522–540 (2015)
51. Svärd, M., Nordström, J.: Review of summation-by-parts schemes for initial-boundary-value problems. J. Comput. Phys. **268**, 17–38 (2014). https://doi.org/10.1016/j.jcp.2014.02.031
52. Toro, E.F., Montecinos, G.I.: Advection-diffusion-reaction equations: hyperbolization and high-order ADER discretizations. SIAM J. Sci. Comput. **36**(5), A2423–A2457 (2014)
53. Virtanen, P., Gommers, R., Oliphant, T.E., Haberland, M., Reddy, T., Cournapeau, D., Burovski, E., Peterson, P., Weckesser, W., Bright, J., van der Walt, S.J., Brett, M., Wilson, J., Jarrod Millman, K., Mayorov, N., Nelson, A.R.J., Jones, E., Kern, R., Larson, E., Carey, C., Polat, I., Feng, Y., Moore, E.W., VanderPlas, J., Laxalde, D., Perktold, J., Cimrman, R., Henriksen, I., Quintero, E.A., Harris, C.R., Archibald, A.M., Ribeiro, A.H., Pedregosa, F., van Mulbregt, P.: SciPy 1.0 contributors: SciPy 1.0: fundamental algorithms for scientific computing in python. Nat. Methods **17**, 261–272 (2020). https://doi.org/10.1038/s41592-019-0686-2
54. Yang, J.: Nonlinear Waves in Integrable and Nonintegrable Systems. SIAM, Philadelphia (2010)
55. Zeifang, J., Schütz, J., Kaiser, K., Beck, A., Lukáčová-Medvid'ová, M., Noelle, S.: A novel full-Euler low Mach number IMEX splitting. Commun. Comput. Phys. **27**, 292–320 (2020)